TÉCNICO LISBOA

Modelling of the human lens complex under cataract surgery.

Maria Teresa Andrade Santos Leitão Cardoso

Thesis to obtain the Master of Science Degree in

Biomedical Engineering

Supervisors: Professor Paulo Rui Alves Fernandes

Doctor Maria Filomena Jorge Ribeiro

Examination Committee

Chairperson: Professor Fernando Manuel Fernandes Simões

Supervisor: Doctor Maria Filomena Jorge Ribeiro

Members of the Committee: Professor João Orlando Marques Gameiro Folgado

Doctor Carlos Alberto Matinho Marques Neves

October 2018

Acknowledgements

First, I would like to acknowledge my supervisors, Professor Paulo Fernandes and Doctor Filomena Ribeiro, for all the guidance, patience and advice, every time I needed them, especially Professor Paulo Fernandes who in our meetings was always ready to laugh, believed in this work, in my capacities and in my judgement, supported me in giving me a lot of liberty to do what I thought was the best for this work.

I would also like to thank Professor André Castro who helped me principally at the end of this work and will help with the future development of the same.

Thank you to IDMEC for giving me the opportunity to go further with this investigation for another three months.

I would also like to thank all my friends, always ready to lighten up the mood when I was in difficulties or more stressed, they always knew what to say, and especially to my friends who worked in the same workspace as me, for helping me with technicalities, making me laugh and supporting me.

Finally, I want to thank my family who even so far always believed in me, pushed me into the right direction, supported all my decisions and gave me the opportunity to study here, in such an amazing faculty.

Abstract

A cataract is a disease that affects the crystalline, when it loses transparency and becomes opaque, leading to a blurred vision, and in the extreme to blindness. With the aging of population, the incidence and prevalence of cataracts is increasing, as well as the number of procedures performed to remediate to it. The crystalline complex, including the crystalline, the capsular bag, the zonular fibers and the ciliary body, is of extreme importance since it allows the eye to focus objects. Nowadays the most common solution available for cataracts is its complete removal, followed by an implant of an intraocular lens (IOL), turning it into a pseudophakic eye. With the increase of cataract surgeries, an increase in post-operative complications arose, the most serious being posterior chamber IOL dislocation. Computational models of the complete crystalline complex were already built, but none after cataract surgery. In this work, through the software Abaqus®, an axisymmetric Finite Element (FE) Analysis of the crystalline complex during the process of accommodation under cataract surgery, with an IOL implant is proposed, to understand if there is a mechanical influence on post-operative complications. An increase of force and stress in the zonules was verified in the pseudophakic eye compared to the complete eye, that could explain why years after surgery zonules would break leading to an IOL dislocation. The model proposed in this work is innovative in this field and would be a good complement for the already existing work about the crystalline complex.

Keywords: cataract, intraocular lens, axisymmetric, membrane, capsular bag, zonular fibers

Resumo

A catarata é uma opacificação do cristalino, que perde transparência levando a uma visão turva e, quando não tratada a tempo, a cegueira. Com o envelhecimento da população, a incidência e prevalência das cataratas está a aumentar, bem como o número de cirurgias para as tratar. O complexo do cristalino, que inclui o cristalino, o saco capsular, as zónulas e o corpo ciliar, é de extrema importância sendo que é responsável pela capacidade do olho a focar objetos. Hoje em dia, a solução mais comum para as cataratas é a remoção da mesma, seguida de um implante de uma lente intraocular (LIO) para substituir o cristalino e as suas funções, deixando o olho num estado pseudofáquico. Com o aumento de procedimentos cirúrgicos efetuados, verifica-se consequentemente um aumento de complicações pós-cirúrgicas, sendo o deslocamento da LIO a complicação mais séria. Alguns modelos computacionais do cristalino completo já foram estudados, mas nenhum depois da cirurgia das cataratas. Neste trabalho apresenta-se um modelo axisimétrico de elementos finitos do cristalino durante o processo de acomodação, antes e depois de cirurgia com implante de LIO, para perceber se há alguma razão mecânica para o deslocamento da LIO ocorrer. Verificou-se um aumento de tensões e de forças nas zónulas pós-cirurgia, o que poderia explicar o porquê de, anos depois da cirurgia, alguns zónulos partirem levando ao deslocamento da LIO. O modelo aqui proposto é inovativo nesta área e apresenta ser um ótimo complemento aos estudos já existentes sobre o complexo do cristalino.

Palavras-chave: catarata, lente intraocular, axisimétrico, membrana, saco capsular, zónulas

Contents

List of Figures

List of Tables

List of Acronyms

3D	Three-dimensional
ACCS	Anterior Capsular Contraction Syndrome
CAX3	3-node linear axisymmetric triangle element
CAX4	4-node bilinear axisymmetric quadrilateral element
CAX4R	4-node bilinear axisymmetric quadrilateral with reduced integration with hourglass control element
CAX6M	6-node modified second-order axisymmetric triangle element
CAX8	8-node biquadratic axisymmetric quadrilateral element
CAX8R	8-node biquadratic axisymmetric quadrilateral with reduced integration with hourglass control element
CCC	Continuous Curvilinear Capsulorhexis
ECCE	Extracapsular Cataract Extraction
FE	Finite Element
ICCE	**I**ntracapsular Cataract Extraction
IOL	Intraocular Lens
MAX1	2-node linear axisymmetric membrane element
MAX2	3-node quadratic axisymmetric membrane element
PCO	Posterior Capsular Opacification
PMMA	Polymethyl Methacrylate
RF	Reaction Force
TF	Traction Force

List of Nomenclature

E_C	Young's modulus of the cortex
E_{CB}	Young's modulus of the capsular bag
E_N	Young's modulus of the nucleus
E_Z	Young's modulus of the zonules
R_{lens}	Length of the major axis of the cortex/Total length of the intraocular lens
$R_{nucleus}$	Length of the major axis of the nucleus
R_{optic}	Radius of the optic of the intraocular lens
R_{total}	Radius of the ciliary body
R_{zon}	Length of the equatorial zonules
RF_Z	Resulting force at the tip of the zonules
S_{CB}	Von Mises stress in the capsular bag
S_{IOL}	Von Mises stress in the intraocular lens
S_Z	Von Mises stress in the zonules
T_{haptic}	Thickness of the haptic of the intraocular lens
T_{lens}	Thickness of the cortex/intraocular lens
$T_{nucleus}$	Thickness of the nucleus
T_{optic}	Thickness of the optic of the intraocular lens
δ	Outward displacement applied at the tip of the zonules
δ_R	Difference in length in the radial direction
δ_T	Difference in length in total lens thickness
Φ_{CCC}	Diameter of the continuous curvilinear capsulorhexis
v	Poisson's ratio

1. Introduction

1.1. Motivation

Cataract is a disease that leads to visual impairment, and eventually to blindness, worldwide. With the aging of population, the incidence and prevalence of cataract is increasing, as well as the number of procedures performed to remediate to it, consequently. Prokofyeva made a literature review in 2013, using data between 1990 and 2009, and concluded that in Europe the prevalence of this disease increased from 5% in population between 52-62 years-old and from 30% for 60-69 years old to 64% in population above 70 years-old (Prokofyeva et al., 2013). In the United States, the same previsions are made. A projection of the prevalence of cataracts has been made for the years 2030 and 2050, with the number of cases going from 38 million to 50 million (National Eye Institute, 2010). Cataract surgery with an intraocular lens (IOL) implantation has been quickly evolving over the years, with the development of new technologies and techniques, such as phacoemulsification and new materials for IOLs, making it a safer procedure than it was a couple of decades ago. Following cataract surgery, few complications can appear, the most serious being posterior chamber IOL dislocation since it leads to more complex surgeries, although it is uncommon (Al-Halafi et al., 2011). The following *in silico* studies shall help understand the mechanics of the IOL dislocation, and study the parameters that could influence this complication, due to their increasing incidence following the increase of procedure performed to remove cataracts.

1.2. The Human Eye Lens Complex

The human eye lens complex is composed by four main components: the capsular bag (or capsule), the crystalline lens (composed by the cortex and the nucleus), the zonular fibers (or zonules) and the ciliary body. This complex, shown in Figure 1.1, is of extreme importance in the human visual system since it allows the eye to focus objects, i.e., to accommodate. The crystalline lens is a transparent and flexible structure enclosed inside a thin membrane with a thickness of about 10 μm, even though Fisher and Pettet

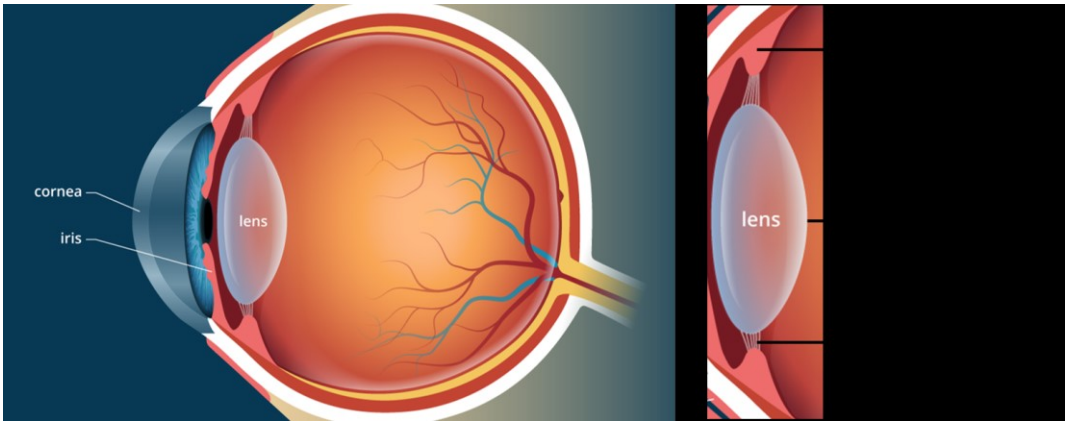

Figure 1.1. On the left: Complete eye structure, with the human lens located behind the iris. On the right: close-up of the crystalline lens complex, with the lens inside the capsular bag and held by the ciliary body through the zonules. Adapated from Heiting, 2017.

(1972) showed it slightly changes with age and position, the capsular bag, and is connected to the ciliary body by the zonular fibers, at the zonular lamella. The zonules are known to be separated in three distinct groups, all around the circumference of the lens: the anterior, the equatorial and the posterior group. They are considered as suspensory ligaments which hold the lens in position, but also reshape it during accommodation.

A few theories about accommodation have risen and were not always in concordance. The most popular one was the Helmholtz's theory (Southall, 1962) that stated that in the unaccommodated (or disaccommodated) state, the lens was held in a state of radial tension by all the zonules. When beginning the process of accommodation, the ciliary body contracted leading to a reduction of tension in the zonular fibers and to an increase of curvature of lens surfaces and optical power, until reaching the fully accommodated state. Opposed to Helmholtz's, stood Schachar's theory (Schachar, 1992) stating that when going from the unaccommodated to the accommodated state, the contraction of the ciliary body lead to an increase of tension in the zonular fibers, i.e., stating that the zonules had a direct effect on this process. In a mechanical point of view, Helmholtz claimed that the stress-free state of the lens complex was when it stood in an accommodated state, with no stresses on the zonular fibers, whereas Schachar stated that this stress-free state occurred in the unaccommodated state. Figure 1.2 shows an eye in the accommodated and in the unaccommodated state.

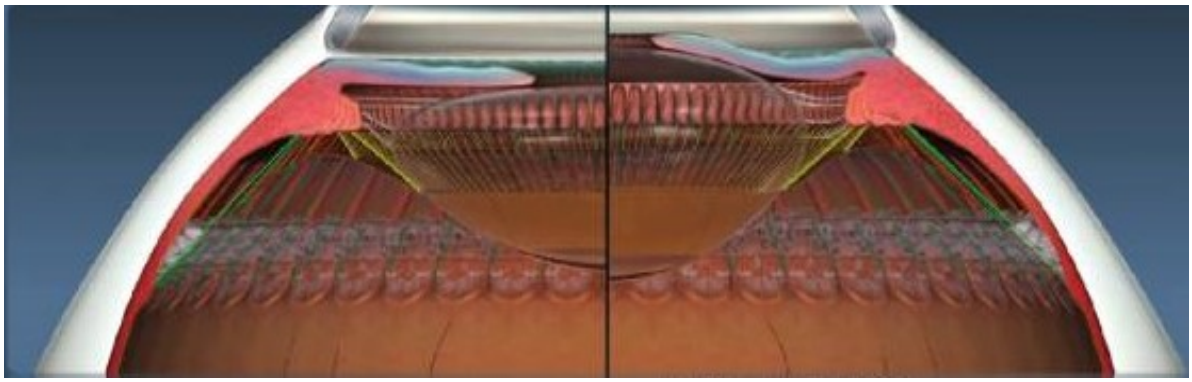

Figure 1.2. View showing half the eye (left) in an unaccommodated state and the other half (right) in an accommodated state. Adapted from Goldberg et al., 2011.

Understanding the mechanisms of accommodation was very relevant in order to study some complications regarding the crystalline lens and its associated structures. The main one, that is going to be discussed in this work, usually occurs in late adult life, when the crystalline lens loses too much transparency and becomes opaque: it is said to be a cataract. This results in the reduction of the transmission of light and in scattering light, leading to a blurred vision, and in the extreme, when not treated in time, to blindness. Nowadays, the most common solution available is the complete removal of the cataract, i.e., of the crystalline lens, followed by an implant of an IOL to replace it (Ascaso & Huerv, 2013). However, if the cataract does not affect everyday activities, it does not need to be operated.

1.3. Objectives

The main objective of this thesis was to propose a mechanical model of the IOL-capsular bag complex after cataract surgery. Furthermore, knowing that late IOL-capsular bag dislocation was one of the most serious problems after this procedure, we aimed to study the stresses in the capsular bag, in the zonular fibers and in the implanted IOL through a Finite Element (FE) Analysis, to understand when did the zonules break and lead to the dislocation of all the complex. Few parameters, as the diameter of the capsulotomy, the traction force on the edge of the capsulorhexis, and materials of the IOL were studied to see if they had an influence on this process and to seek the best configuration to avoid this complication.

1.4. Outline of the Thesis

Besides this first chapter of introduction, this document is divided in five more chapters, presenting a review of the literature about cataract surgery and human lens' models, this work's computational models and methods used, the outcomes obtained and their discussion, and lastly the conclusions.

In the second chapter, a review of the literature is presented, about the evolution of cataract surgery as well as computational eye models that have already been made and their associated properties of the materials.

In the third chapter, the FE lens models, before and after surgery, are described, as well as the lens and IOL's geometry, the materials properties chosen for this study, the construction and design of the FE mesh and the parameters that will be evaluated, for an axisymmetric model.

In the fourth chapter, the validation of the axisymmetric model is described and debated.

In the fifth chapter, the results of stresses for all the models are discussed, i.e., before and after surgery, for the axisymmetric model.

In the sixth and last chapter, the outcomes of the simulations will be discussed, and conclusions will be established, along with the limitations of this work and proposals of its future development.

2. Literature Review

2.1. Evolution of Cataract Surgery

Modern cataract surgery, by extraction, first appeared in the middle of the 18th century, with mainly two types of procedures being performed. The first one, called an intracapsular cataract extraction (ICCE), consisted in the destruction of the zonules and more importantly, in the removal of the capsule through a large incision in the cornea (of about half its circumference), as the cataract was removed as a single piece. Because of the size of the incision, visual recovery remained very difficult. The extracapsular cataract extraction (ECCE) contrasted with the ICCE, since the zonules and the posterior capsule remained untouched, thanks to an additional incision in the anterior capsule. At that time, after removal of the cataract, the incisions were simply sutured, leaving the eye without a lens, i.e., in an aphakic state, resulting in a blurry vision and in trouble focusing on objects, that could only be corrected by very thick eyeglasses or by contact lenses. It was only in the middle of the 20th century that the concept of IOL implantation arose, leaving the eye in a pseudophakic state after the surgery. Nowadays, ECCE by phacoemulsification is the method of predilection of most surgeons, since it allows the extraction of the cataract through a very small incision (Ascaso & Huerv, 2013).

ECCE by phacoemulsification begins with few small incisions in the cornea, to allow the insertion of the surgical instruments into the anterior chamber of the eye. A viscoelastic substance is then injected into the chamber to avoid its collapse. A complete incision of the anterior capsular bag (anterior capsulotomy, involving the removal of a part of the capsule) is performed so the crystalline can be removed. To separate the lens nucleus and cortex from the capsule, a fluid wave is created by the injection of a fluid (hydrodissection). The process of phacoemulsification can finally take place by sculpting the nucleus with an ultra-sound probe, until it cracks once. By rotating the lens and repeating this procedure, the lens will be cracked in four quadrants. These are then emulsified and aspirated one after another, with attention not to puncture the posterior capsular bag. To avoid capsular bag collapse during IOL insertion, a viscoelastic substance is injected in the capsule. After the IOL has been implanted in the desired position, the viscoelastic substance is removed, letting the capsular bag shrink and seal itself to the IOL. Since the incisions on the cornea are very small, they do not need any kind of sutures and self-seal (Ascaso & Huerv, 2013).

2.1.1. Capsulotomy

Through the years, the capsulotomy has tremendously evolved, from a rough opening to continuous curvilinear capsulorhexis (CCC). This evolution has a big impact on preventing some serious complications of ECCE cataract surgery, such as posterior capsular opacification (PCO), and on stabilization and fixation of the IOL inside the capsular bag. Before IOL introduction and after the invention of phacoemulsification, capsulotomy was only made to extract the lens nucleus and was therefore a large rough opening (Christmas tree capsulotomy). Few years later, Richard P. Kratz believed that a symmetrical capsular opening was easier and better to increase the performance of the phacoemulsification (Packard, 2015) and created the

can-opener capsulotomy, made by multiple small cuts (Figure 2.1 (A)). The problem with the latest, when IOL were introduced, was that this opening could not guarantee that the IOL was correctly placed in the capsular bag, and not in the sulcus, or if it would stay correctly fixed (Packard, 2015). These uncertainties disappeared with the introduction of the CCC (Figure 2.1 (B)).

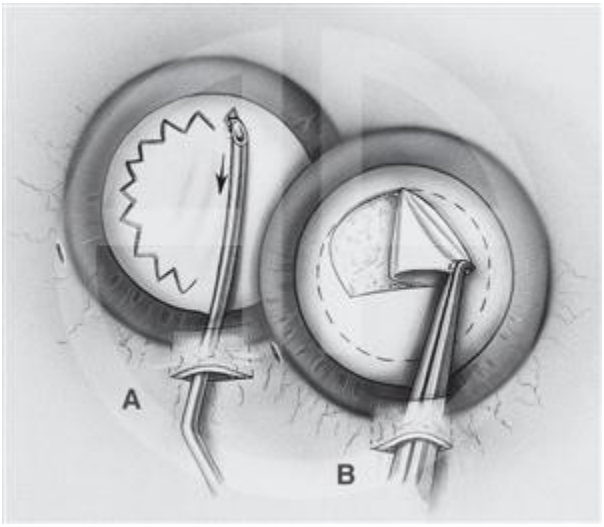

Figure 2.1. Example of a can-opener capsulotomy (A) and a continuous curvilinear capsulorhexis (B). Figure from © 2018 American Academy of Ophthalmology.

Furthermore, to decrease the prevalence of PCO, a proper overlapping of the capsular bag edge, with the IOL is of extreme relevance, after capsulotomy (Packard, 2015). The size, localization and shape of the capsulorhexis has been shown to have a great impact on the development of PCO after cataract surgery. A study published by Langwińska-Wośko et al., comparing small (65-80 % of the diameter of the IOL optic) and large (81-98% of the diameter of the IOL optic) capsulorhexis, with a regular or irregular shape, on the center of the optic or a bit out of it, concluded that small capsulorhexis diameter, centered and with a regular cut is the best option to decrease the risks of PCO to null or mild, i.e., with no need of further surgery (Langwińska-Wośko et al., 2011).

Moreover, some studies have already shown that a small CCC would lead to an increased probability in developing fibrosis and shrinkage of the capsular bag, complication known as anterior capsule contraction syndrome (ACCS). Since ACCS is the result of myofibroblastic transformation of the capsular bag on the IOL, a smaller CCC gives a wider area of contact of the capsule with the IOL. (Gimbel et al., 2005) Following the development of ACCS, an IOL-capsular bag dislocation has more probability of occurring.

2.1.2. Intraocular Lenses

The IOL material and design have also both an influence on these complications. An IOL must follow certain specifications in terms of biocompatibility, mechanical properties and optical performances, depending on the site of fixation. In this work, only the posterior chamber lenses, i.e., in the capsular bag, will be mentioned. Since cataract surgery is performed more and more at earlier stages of life, biocompatibility is

crucial to avoid complications for many years. Regarding their mechanical properties, IOLs should be compressible to not damage the capsular bag when accommodated and have shape memory when unaccommodating (Sheehan, 2012).

Polymethyl methacrylate (PMMA) lenses were the first ones ever used in a cataract surgery with IOL implantation (Nguyen & Werner, 2017). But, since PMMA was a very rigid material, these IOL were not foldable and required a larger corneal incision (at least as big as the lens) and suture to close the wound (Scholtz et al., 2014), leading to a longer recovery time after surgery. With the evolution of small incision cataract surgery, PMMA lenses are nowadays rarely used, despite their excellent biocompatibility. To overcome the rigidity of PMMA IOLs and to avoid large corneal incisions, silicone lenses were produced and were the first foldable IOLs implanted during cataract surgery. Silicone IOLs are generally avoided in patients with a high risk of uveitis, diabetic retinopathy or retinal detachment, since these complications may require a vitrectomy surgery with silicone oil replacement, very adherent to silicone IOLs, eventually leading to visual disturbance or visual loss for the patient (Trivedi et al., 2002). More recently, acrylic foldable IOLs with better biocompatibility appeared. They are made of a modified PMMA, with a substituted side-chain molecule and can be made hydrophilic or hydrophobic, making them more robust than PMMA IOLs and with less after surgery complications than silicone IOLs.

Posterior chamber lenses, as shown in Figure 2.2, for in-the-bag fixation can be described as single-piece or multi-piece, i.e., made of one material or of (generally) different materials for the haptics and the optics. Single-piece IOLs, also known as one-piece IOLs, have two main configurations: plate lenses or open loop, i.e., with an optic and haptics. For IOLs with haptics, PMMA is commonly used to give rigidity to resist external forces, e.g., extreme ACCS (Nguyen & Werner, 2017).

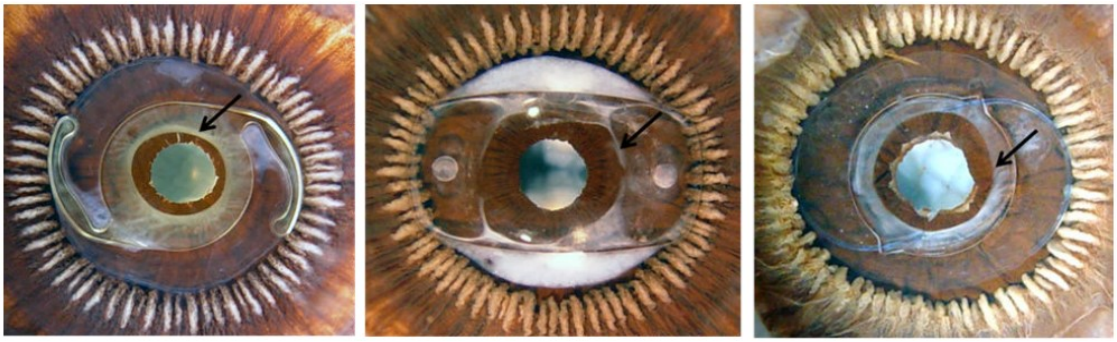

Figure 2.2. Few examples of different designs of posterior capsule in-the-bag IOLs. The arrows show the capsulotomy in each eye. On the left, single piece IOL. In the middle, plate IOL. On the right, multi-piece IOL.. Adapted from Nguyen & Werner, 2017.

Since PCO is the most common post-operative complication, various studies tried to link this phenomenon with the IOL design and material and to find a solution to diminish it. Since the main precursor of PCO is the Soemmering's ring, that forms in the anterior capsule and then migrates to the posterior capsule, it is possible to create a physical barrier to enhance the contact between the capsular bag and the IOL with a

square optic edge (Figure 2.3), and consequently reduce the migration of these cells. Furthermore, to reduce cellular proliferation, the use of a biocompatible IOL is recommended (Nguyen & Werner, 2017).

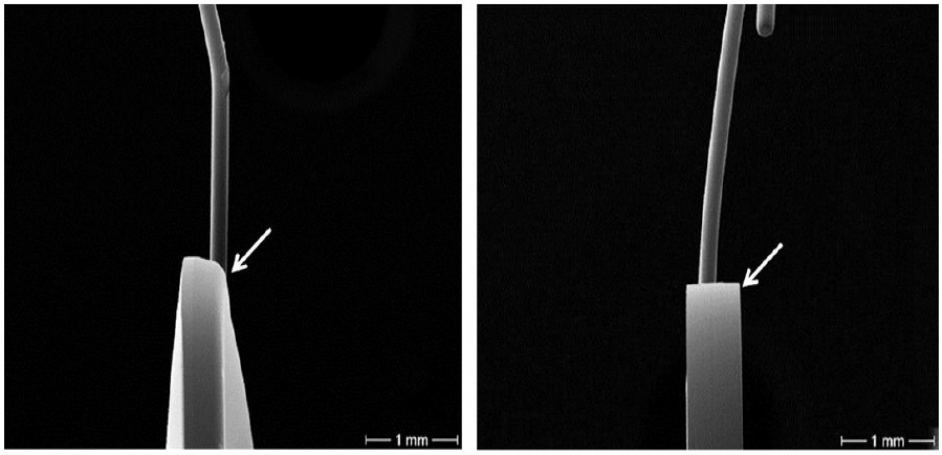

Figure 2.3. Two types of multi-piece IOLs with different optic edges. On the left, round optic edge. On the right, square optic edge. Adapted from Nguyen & Werner,2017.

The size and material of the IOL has also been suggested to have an impact of the development of IOL-capsular bag dislocation or shrinkage. A plate-haptic silicone IOL induces more capsule contraction (Werner et al., 2000), as well as one-piece acrylic IOLs that may induce more fibrosis and less haptic resistance to capsule contraction (Izak et al., 2004). On the other hand, three-piece hydrophobic acrylic IOLs may reduce capsular contraction thanks to greater haptic rigidity and less capsular fibrosis (Werner et al., 2000).

2.1.3. Post-Surgery Complications

Even though cataract surgery has a very low rate of post-operative complications, with 90% of the patients reporting better vision after the procedure (Brown et al., 2013), some of them may require further treatment or even surgery to avoid serious problems, such as blindness in the extreme cases.

The most common is PCO, where residual lens epithelial cells migrate to the posterior capsule, increasing opacity and impairing the vision of the patient (Meacock et al., 2003), turning it worse than before the surgery in some cases. The main precursor of PCO is the formation of a Soemmering's ring, result of residual E cells following the disruption of the anterior capsule (Nguyen & Werner, 2017). Fortunately, if visually significant, the treatment is effective and painless thanks to the YAG laser, allowing a posterior capsule capsulotomy. The laser removes the central zone of the hazy posterior capsule, without the need of making an incision.

Anterior capsular contraction syndrome (ACCS) or rhexis contraction, is a condition that often happens following cataract surgery since it is the natural fibrosis of the capsulotomy, but is only considered as a complication when it reaches the visual axis, obscuring vision. Fibrosis of the capsular bag is the result of myofibroblastic transformation, leading to the contraction of the anterior capsulotomy towards the center of its opening, creating a centripetal force. In extreme cases, if this centripetal force is higher than the

centrifugal force exerted by the zonules, they might ultimately break and cause IOL dislocation, tilt or decentration (Hudish et al., 2017). For an early stage of ACCS, with obstruction of the vision but no IOL-related complication, the general treatment for this symptom is also the use of the YAG laser.

IOL-capsular bag complex spontaneous dislocation or subluxation is an uncommon but most serious complication after phacoemulsification procedure. In fact, this dislocation first leads to a loss of vision of the patient, and further leads to the IOL being mobile in the vitreous cavity or being in contact with the retina, causing consequently retinal detachment, glaucoma, uveitis or cystoid macular edema (Al-Halafi et al., 2011)(Rusu et al, 2014). A large population-based cohort study observed a cumulative risk of IOL-capsular bag complex dislocation going from 0.1% at 5 years after surgery to 1.7% at 25 years after (Pueringer et al., 2011). Two types of dislocation exist: early and late cases. The first one often occurs after posterior or equatorial capsule rupture or because of zonular dehiscence, in three-months' time after surgery. It is frequently a result of damage made during the procedure, such as improper IOL fixation in the capsular bag. The second one occurs after three months following the surgery and is generally related with progressive zonular weakness and extreme ACCS. It differs from early dislocation mainly because the IOL is properly fixed and the dislocation also involves the capsular bag. To keep the IOL-capsular bag complex in the correct position after its dislocation, it must be sutured or fixed on the iris. Another surgical procedure, called explantation surgery, consists in the complete removal of the complex with the insertion of a new lens, fixed on the iris. This last one has its downsides since it requires a big differentiation in the surgeon and can eventually lead to more complications.

2.2. Finite Element Models

The information about the mechanical properties of the lens tissues (capsular bag, nucleus and cortex of the crystalline, and zonular fibers) was limited and disperse. Even though several *in vivo* studies targeted these tissues, there is a lack of consensus about stiffness and other values that are relevant to build a computational model of the human lens complex. The brief literature review in this chapter will resume the state of the art of FE models of the human lens complex.

From 1999 to 2002, Burd et al. built the firsts FE computational model of the human crystalline. In the beginning of their investigation, they aimed to compare the two fundamental accommodation theories, Helmholtz's and Schachar's. The lens nucleus and cortex were modelled as linearly elastic incompressible materials, since there was no data to help achieving a more complex model, the capsular bag as a membrane and the zonules, only the equatorials, as a traction force, all in an axisymmetric geometry. Figure 2.4 depicts the geometry of the model described by Burd et al. in their first work (1999). The capsule had a constant thickness and a variable Young's modulus. The analysis used an energy method based on linear theory, to compute displacements after the zonular traction was applied. The linear theory ignored the non-linear terms that are of extreme importance to correctly understand big displacements in membranes (Burd et al., 1999). They concluded that for young eyes, the Helmholtz theory was the more correct to model the crystalline. In 2002, with the purpose of studying the mechanisms of presbyopia, i.e., a disease where the

crystalline loses stiffness leading to a decreased accommodating power, Burd et al. continued their first work. One major difference with their previous study, was that the three sets of zonules were considered as three membrane annular sheets, connecting at a single point, with different axial stiffnesses to simulate the different density of zonules that existed *in vivo*. The capsular bag had a varying thickness but was still modelled as a membrane with axial stiffness but no bending stiffness. Dislocation was applied at the intersection of the sets of zonules. The outcomes of this analysis were that in the fully disaccommodated state of the crystalline, a radial force between 0.08 N and 0.1 N was being applied through the zonules (Burd et al, 2002).

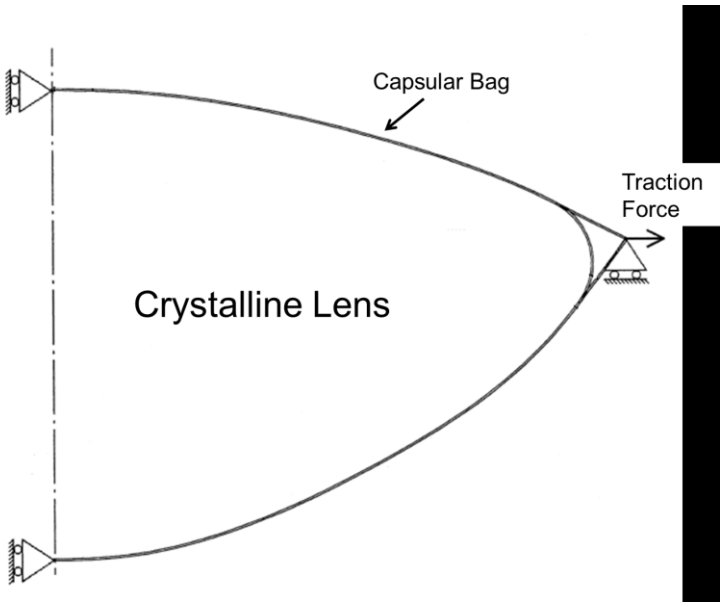

Figure 2.4. Axisymmetric finite element model of the crystalline lens, the capsular bag and traction force used to mimic the zonules. Adapted from Burd et al., 1999.

In 2005, Le also modelled an axisymmetrical human lens to deepen the understanding of the optical power and displacement of the human lens during accommodation. All the components of the eye were defined as orthotropic nearly incompressible closed shells. The capsule had a varying Young's modulus, composed of shell elements, and various elastic moduli were tested for the cortex and nucleus. A single line-load at the equator representing the zonules with an outwardly displacement, as well as three line-loads at the anterior, equatorial and posterior sites were tested. The model with only the equatorial zonules showed a better performance, with an increased optical power (Le, 2005).

One year later, with the goal of studying the lens with an improved shape during accommodation, Chien et al. performed an analysis on four axisymmetric models, with hyper-linearly elastic shell capsules. Only the equatorial zonules were represented, as a line-load. Their new geometrical model showed very similar behaviors of steepening and flattening of the lens after achieving disaccommodation, compared with some *in vivo* experiments (Chien et al., 2006). In the same year, Hermans et al. tried to estimate the influence of different configurations of the zonules on the forces acting on the crystalline during all the process of accommodation. The material properties were all modelled as Burd et al. but with specific values of Young's

modulus found in various studies, and the zonules were described as forces, not needing any material property, consequently. The initial state of the model, i.e., a fully accommodated crystalline, assumed no force acting on it. The results obtained for each experience showed a total magnitude of zonular force of approximatively 0.08 N, regardless of the configuration of the zonules (Hermans et al., 2006).

Weeber & van der Heijde used the shape of an *in vivo* accommodated lens to describe the deformations occurring in it during the process of accommodation. An axisymmetric model was built, with all materials being linear elastic isotropic. The three sets of zonules were represented and were stretched radially until an increase of 7% of the lens diameter was achieved. The capsular bag and zonules had a constant Young's modulus, whereas the cortex and nucleus (modelled as only one entity) had a variable one. They confirmed that the bigger deformations occurred on the axial direction, i.e., on the zonular traction direction, in the lens' central area (Weeber & van der Heijde, 2008).

In a three-dimensional computational work, Lanchares et al. performed a numerical simulation to further understand and test different mechanical properties of the human crystalline than the ones used in previous studies. All this process was divided in two steps. The first one was the estimation of the zonular force during accommodation and the second one was to correlate material properties of all the components with age, based on the force computed earlier. The zonular force was assumed to remain constant throughout life on the basis that the ciliary muscle remained functional, with no loss of capacity, in the same time. Thanks to the three-dimensionality of the problem, a hyperelastic anisotropic capsule with a variable thickness could be introduced, on the basis that it had a non-linear pseudoelastic behavior over finite strains. The other materials were modelled as in previous works, with an isotropic cortex and nucleus. A radial direction of deformation and the three sets of zonules were considered, with three different width bands as the zone of insertion. A resulting force of 0.078 N was computed to completely disaccommodate the eye, a value very similar to the ones found by Burd et al. (2002) and Hermans et al. (2006) (Lanchares et al., 2012).

In 2016, Bahrami et al. considered in an axisymmetric model that the cortex and nucleus had a variable Young's modulus from its center to its surface, based on *in vivo* measurements performed on a 27-years-old lens. All the elements of the model were modelled as quasi-incompressible materials, with the capsular bag having a variable thickness and the cross-section of the zonules being a continuous plane. With this representation of the zonules, the plane covered a range of insertion points to the ciliary body and to the capsular bag, representing the three sets of zonules at the same time. This study was performed to deepen the understanding of the changes of the gradient refractive index of the human lens during accommodation (Bahrami et al., 2016).

More recently, Wang et al. presented an axisymmetric parametric study with different configurations of zonular angles (for all three sets of zonules) and material properties, to show the relevance and influence of all the parameters involved in a computational simulation on the outcomes obtained. All materials in the model were considered as linearly elastic quasi-incompressible isotropic, with constant Young's moduli. The capsular bag was designed with shell elements whereas the zonules were with shell elements with

membrane stiffness, as they were considered as continuous sheets. Figure 2.5 shows the model built by Wang et al. Displacement was applied at the tip of the zonules, where they should be anchored to the ciliary body, in concordance with an MRI study stating that the maximal change in ciliary body diameter was from 1 to 1.2 mm. They concluded by showing that different configurations of zonular angles and different capsule thickness have a great impact on the shape of the crystalline during accommodation, even though it was still difficult to state which was the best configuration due to the lack of *in vivo* information about the process of accommodation, and real values of Young's moduli (Wang et al., 2017).

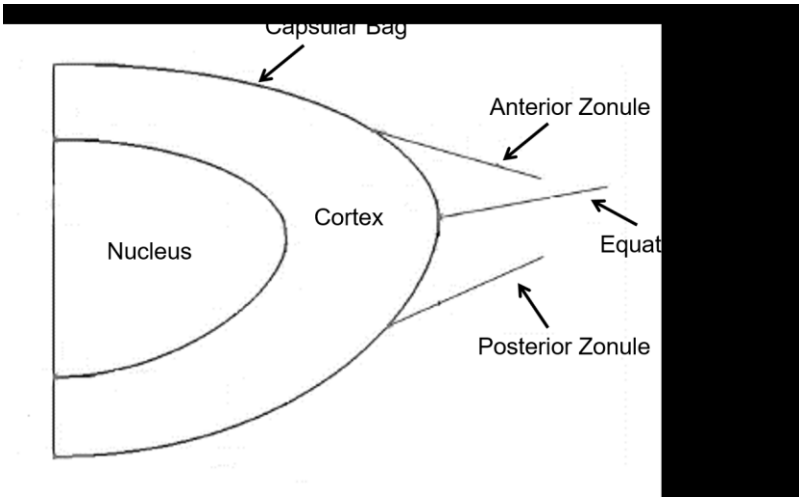

Figure 2.5. Axisymmetric finite element model of the crystalline lens (nucleus and cortex), the capsular bag and the three sets of zonules (anterior, equatorial and posterior). Adapted from Wang et al., 2017.

Most of the published work agreed on one point: the available information about the mechanical properties or behavior of the human lens *in vivo* was very scarce and did not allow anyone to do a complete and perfect computational replica of this complex, to study its mechanisms. The mechanical behavior of the lens during accommodation and disaccommodation not only depended on its mechanical properties, but also on its detailed geometry. This last aspect involved a different limitation, since there was no complete geometric description of a specific lens, leading to the construction of a single model based on a small number of different sources. The part of the crystalline complex with less information, about its geometric arrangement and mechanical properties was the zonular fibers, with very few reports about their arrangement around the crystalline. If this field of study is to be further developed, i.e., numerical modelling of the study of the process of accommodation in the human lens, new high quality *in vivo* mechanical and geometric data needs to become available. A summary of the mechanical properties used in related works using computational models of the human lens is depicted in Table 2.1. The specific mechanical properties described in Table 2.1 are the Young's moduli of the capsular bag (E_{CB}), the cortex (E_C), the nucleus (E_N) and the zonules (E_Z), as well as their respective Poisson's ratio (v) or the line-load (RF_Z) used to model the zonules.

*Table 2.1. Summary of the mechanical properties used in related works using computational models of the human lens. The * means that some specific values where not mentioned in the works.*

Mechanical Properties	Author	Mechanical Properties	Author
E_{CB} = 5 MPa, v = 0.47 E_C = 0.6-3 kPa, v = 0.49 E_N = 0.6-3 kPa, v = 0.49 E_Z = 10 MPa, v = *	Bahrami et al., 2016	E_{CB} = *, v = * E_C = *, v = * E_N = *, v = * RF_Z = 0.078 N	Lanchares et al., 2012
E_{CB} = *, v = 0.47 E_C = *, v = 0.47 E_N = *, v = 0.47 RF = *	Burd et al., 1999	E_{CB} = 0.75-1.5 MPa, v = 0.47 E_C = 0.05-0.8 kPa, v = 0.49 E_N = 0.05-0.8kPa, v = 0.49 E_Z = 1.5 MPa, v = 0.49	Le, 2005
E_{CB} = 1.5-6 MPa, v =0.47 E_C = 3.42 kPa, v = 0.49 E_N = 0.547 kPa, v = 0.49 E_Z = *, v = *	Burd et al., 2002	E_{CB} = 0.85-22.5 MPa, v = 0.47 E_C = 3.42 kPa, v = 0.49 E_N = 1.27 kPa, v = 0.49 E_Z = *, v = *	Liu et al., 2015
E_{CB} = 1.5 MPa, v = 0.47 E_C = *, v = * E_N = *, v = * RF_Z = *	Chien et al., 2006	E_{CB} = 4.9 MPa, v = 0.47 E_C = 3.7 kPa, v = 0.47 E_N = 0.6 kPa, v =0.47 E_Z = 0.35 MPa, v = 0.47	Wang, 2017
E_{CB} = 1.27 MPa, v = 0.47 E_C = 3.42 kPa, v = 0.49 E_N = 0.547 kPa, v = 0.49 Zonules not modelled	Hermans et al., 2006	E_{CB} = 1.5 MPa, v = 0.47 E_C = 6.25-108.5 kPa, v = 0.5 E_N = 6.25-108.5 kPa, v =0.5 E_Z = 0.35 MPa, v = 0.47	Weeber et at., 2008

3. Materials and Methods

Since the values of the properties of all the materials were very different, and there is still no complete consensus on what type of material to use for either the capsular bag or the zonules, a first set of experiences was made in a computational FE axisymmetric model in Abaqus®, to understand how different materials reacted. The axisymmetric model helped us achieve a three-dimensional-like (3D) result with less computational complexity, using a simple cross-section of the human lens, since the loading conditions are axially symmetric.

3.1. Lens and IOL's Geometry

The first model built in Abaqus® represented the capsular bag, the cortex, the nucleus and the equatorial zonules of the human lens complex, as shown in Figure 3.1. The crystalline, i.e., the cortex and nucleus, had both a perfect ellipsoid shape, with the coordinates of the major ($R_{nucleus}$ and R_{lens}, for the nucleus and cortex, respectively) and minor axis (corresponding to the thickness of the lens, T_{lens}, and to the thickness of the nucleus, $T_{nucleus}$) adapted from the radii used by Lanchares et al. (2012) in their work. Based in a linear regression by Burd et al. (2002) it was also possible to compute the radius of the ciliary body (R_{total}), and consequently to compute the length of the equatorial zonules (R_{zon}) to use in this work. The capsular bag had the same outline as the cortex, to fit perfectly around it. The cortex and nucleus were modelled as solid homogeneous closed shells, whereas the capsular bag and the zonules as membranes, with constant thicknesses of 10 μm (Liu et al., 2015) and 40 μm (van Alphen & Graebel, 1991), respectively.

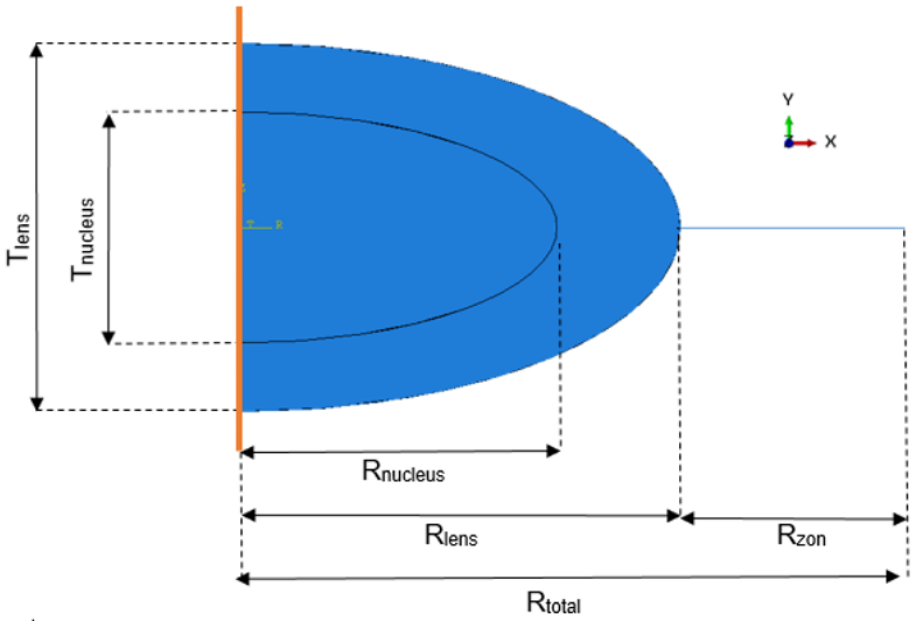

Figure 3.1. Geometry of the eye (nucleus, cortex, capsular bag and zonules) before cataract surgery. The orange line represents the axis of symmetry.

The following models of pseudophakic eyes after cataract surgery, had an IOL replacing the cortex and nucleus of the crystalline after their extraction, and differed in their geometry in the diameter of the capsulorhexis (Φ_{ccc}). As Langwińska-Wośko (2011) proved that small ones had great impact on the development of PCO after surgery, it was interesting to see if their diameter could also have an impact on the IOL-capsular bag dislocation. For this purpose, pseudophakic eyes with small and large capsulorhexis were modelled, i.e., with 72.73% and 81.82% of the diameter of the IOL optic, respectively. Since the models were built axisymmetrically, the capsulorhexis could only be a continuous curvilinear capsulorhexis. The cross-section of the lens that was drawn for this axisymmetric model was based on the cross-section geometry of a one-piece IOL (Alcon SN60WF) described by Sheehan et al. (2012), and is described in Figure 3.2. R_{optic} corresponded to the radius of the optic of the lens, T_{optic} to the thickness of the optic and T_{haptic} to the thickness of the haptics.

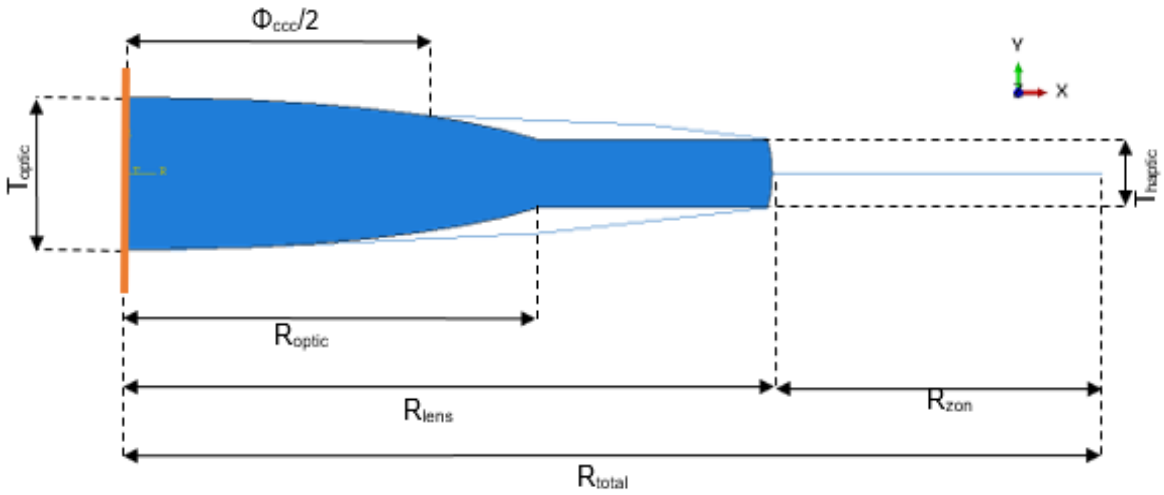

Figure 3.2. Geometry of the pseudophakic eye (IOL, capsular bag and zonules) after cataract surgery. The orange line represents the axis of symmetry.

All the exact dimensions of the model are described in Table 3.1, in mm, for the eye before surgery, and the pseudophakic one with a one-piece IOL implantation.

Table 3.1. Exact dimensions, in mm, of each variable of the crystalline complex before and after undergoing cataract surgery with IOL implantation.

R_{total}	R_{lens}	R_{zon}	$R_{nucleus}$	R_{optic}	T_{lens}	$T_{nucleus}$	Φ_{ccc}	T_{optic}	T_{haptic}
6.5	4.3	2.2	3.1	2.75	3.6	2.26	4.0/4.5	0.96	0.43

3.2. Material Properties

Based on previous studies (Wang et al., 2017)(Weeber & van der Heijde, 2008), all materials of the human crystalline were defined as linear isotropic and quasi-incompressible. In Table 3.2, the mechanical properties of the materials used in these simulations are shown, i.e., their Young's moduli and Poisson's ratio. The parameters of the cortex and the nucleus were based on the study of Wang et al. (2017) and the

capsular bag and zonules based on Weeber & van der Heijde (2008). Three different materials were tested for the one-piece IOL, hydrophilic acrylic, hydrophobic acrylic and PMMA, since they are the most used nowadays. The mechanical properties of those materials came from an experimental study performed by Bozukova et al. (2015).

Table 3.2. Mechanical properties of the crystalline complex before and after surgery.

	Young's Modulus (MPa)	Poisson's Ratio
Cortex	0.0037	0.47
Nucleus	0.0006	0.47
Capsular Bag	1.5	0.47
Zonules	0.35	0.47
Hydrophilic Acrylic	3.911	0.39
Hydrophobic Acrylic	5.829	0.39
PMMA	3000	0.39

3.3. Loads/Boundary Conditions/Interactions

The accommodation process was first simulated using the model of accommodation proposed by Helmholtz (Southall, 1962), with the accommodated state of the lens defined as the stress-free state of the model. Then, to mimic the disaccommodation of the crystalline, an outward displacement (δ) of 0.5 mm, was applied at the tip of the equatorial zonule, where it should be anchored in the ciliary body, that had a maximal change in diameter between 1 mm and 1.2 mm (Wang et al., 2017). Furthermore, for the pseudophakic eye, to simulate the centripetal force towards the center of the opening of the capsulorhexis, a concentrated traction force (TF) was applied. Since no *in vivo* values for this force were found in the literature, few cases were studied, with forces going from zero to values bigger than the reaction force at the zonules. An important aspect to highlight in axisymmetric models, was that prescribed nodal loads or reaction forces were the total values of these loads or forces, integrated along the circumference, around the axis of symmetry. In Figure 3.3 the loading/displacement cases are shown.

In axisymmetric models, there were automatic boundary conditions defined on the axis of symmetry (Y-axis) that constrained the nodes lying on it in the X-direction, i.e., they can only move up- or downward. In light of that, the only part that needed to be manually constrained was the equatorial zonule, that could only be moved in the X-direction, in all the models, before and after cataract surgery.

The interactions occurring between the capsular bag and the crystalline cortex, were based on the assumptions made by Bassnett et al. (1999) saying that the attachment of one to another is strong enough to resist all forces created during the process of accommodation, leading us to assume a tie between both of these components. Since the capsular bag sealed itself to the IOL after surgery, a tie was also considered between the IOL and the capsule (Ascaso & Huerv, 2013).

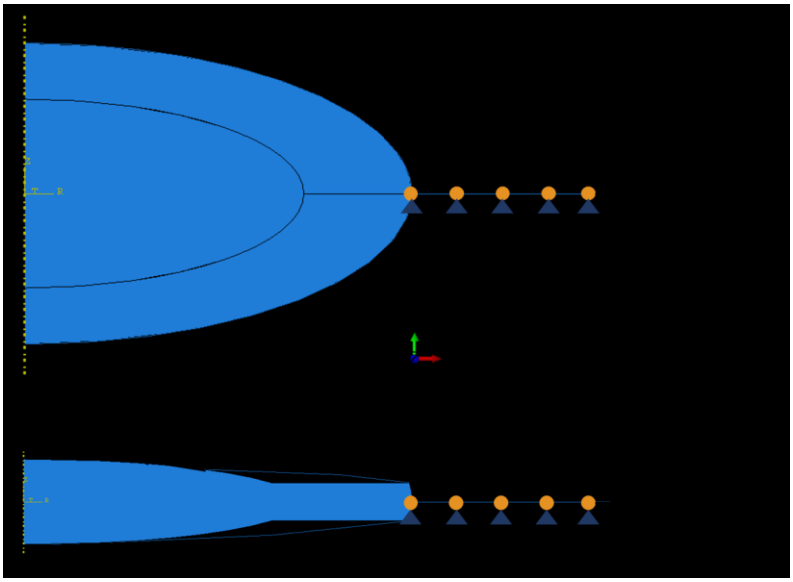

Figure 3.3. Displacement and loads applied to the models. Above: only the radial displacement (δ) is applied at the tip of the zonules for the complete crystalline model. Below: an additional traction force (TF) is applied at the edge of the capsulorhexis for the pseudophakic models.

3.4. Description of Models

With the purpose of studying stresses in the capsular bag, in the zonules and in the IOLs, the change in length in the radial direction (in the X direction) and the resulting forces at the tip of the zonules (RF), a set of 25 models of pseudophakic eyes were built. Since no such FE models were found in the literature, it was important to study the variation and influence of few parameters, such as diameter of the capsulorhexis, the IOL material and the traction force exerted at the opening of the capsulorhexis, on the model. Considering the eye before surgery as *M1*, the features of all the other models are summed up in Table 3.3. For the traction force, since there was no available information on its values *in vivo*, some hypothetic values were tested based on the resulting force at the tip of the zonules when no traction force was applied, with smaller, equal or higher values than this RF. In Table 3.3, the RF*x* corresponds to the resulting force computed in model *Mx*.

Table 3.3. Summary of all the pseudophakic models used in the simulations, differing in the diameter of the capsulorhexis, their IOL materials and traction forces (TF) at the opening of the capsulorhexis.

Name	Φ_{ccc}	IOL Material	TF (N)
M 2.1	4	Hydrophilic acrylic	0
M 2.1	4	Hydrophobic acrylic	0
M 2.3	4	PMMA	0
M 3.1	4.5	Hydrophilic acrylic	0
M 3.2	4.5	Hydrophobic acrylic	0
M 3.3	4.5	PMMA	0
M 4.1	4	Hydrophilic acrylic	0.7
M 4.2	4	Hydrophobic acrylic	0.7
M 4.3	4	PMMA	0.7
M 5.1	4.5	Hydrophilic acrylic	0.7
M 5.2	4.5	Hydrophobic acrylic	0.7
M 5.3	4.5	PMMA	0.7
M 6.1	4	Hydrophilic acrylic	RF2
M 6.2	4	Hydrophobic acrylic	RF3
M 6.3	4	PMMA	RF4
M 7.1	4.5	Hydrophilic acrylic	RF5
M 7.2	4.5	Hydrophobic acrylic	RF6
M 7.3	4.5	PMMA	RF7
M 8.1	4	Hydrophilic acrylic	0.15
M 8.2	4	Hydrophobic acrylic	0.15
M 8.3	4	PMMA	0.15
M 9.1	4.5	Hydrophilic acrylic	0.15
M 9.2	4.5	Hydrophobic acrylic	0.15
M 9.3	4.5	PMMA	0.15

4. Validation

The original model had a capsular bag composed of membrane elements for all the simulations, but since various studies used shell elements to define the capsule, another model was built to compare both properties and understand if it had a great influence on the model.

To validate the choice of the mechanical properties of the different materials of this eye model, a first simulation with the eye before the surgery, undergoing the process of accommodation, was studied and compared with literature models.

4.1. Mesh Convergence Study

The convergence study of the FE mesh was based on varying the size of the elements and the number of nodes for the same-size element. Since different parts of the model were made of different type of elements, there was a necessity to perform a differentiated convergence study, instead of performing a global one. To do so, Von Mises stress values in three nodes from different parts were compared, to ensure the validity of the results within each different mesh used. The mesh of the cortex and nucleus was firstly built with 4-node bilinear axisymmetric quadrilateral elements (CAX4), the capsular bag and zonules with 2-node linear axisymmetric membrane elements (MAX1) and the IOL with 4-node bilinear axisymmetric quadrilateral with reduced integration with hourglass control elements (CAX4R) and some 3-node linear axisymmetric triangle elements (CAX3). These elements allowed an easy conversion to quadratic elements for each component. The cortex and nucleus were built with 8-node biquadratic axisymmetric quadrilateral elements (CAX8), for the capsular bag and zonules 3-node quadratic axisymmetric membrane elements (MAX2) and for the IOL 8-node biquadratic axisymmetric quadrilateral elements with reduced integration with hourglass control (CAX8R) and some 6-node modified second-order axisymmetric triangle elements (CAX6M).

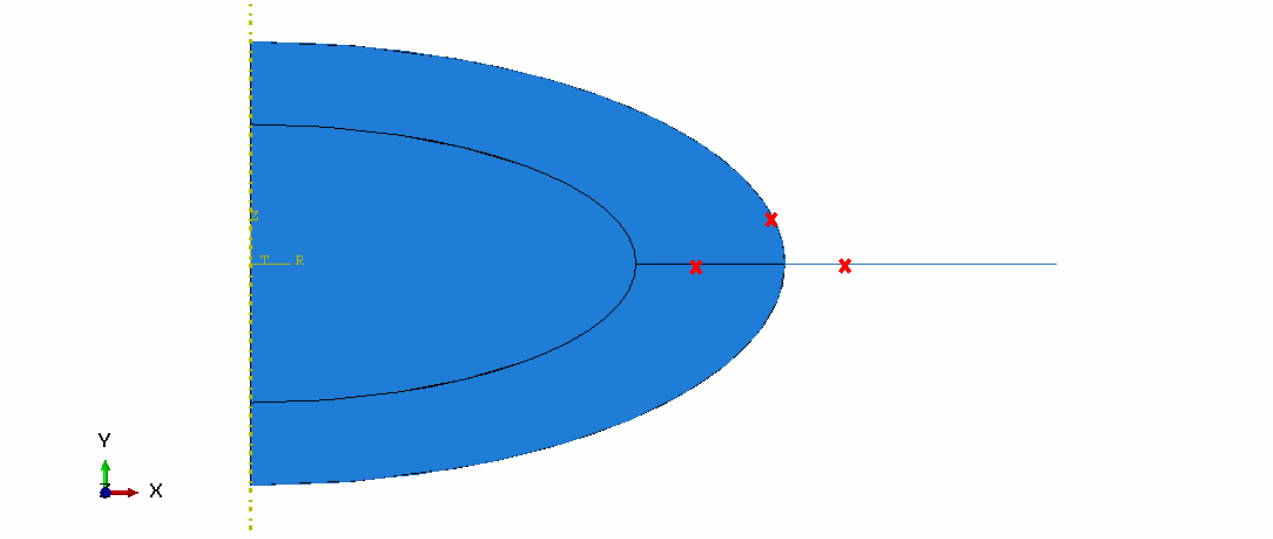

Figure 4.1. Nodes used in the convergence study of the mesh.

For the simulations performed with linear and quadratic elements, they both converged for the same number of elements, i.e., for the same elements size, and for the same value of stress even though the model with quadratic elements had more nodes. Given that outcome, to decrease complexity and computational weight, all the following simulations were carried out with meshes with linear elements. The nodes studied in this convergence study located in the capsular bag, in the zonules and in the cortex of the crystalline are depicted in Figure 4.1.

The values of the von Mises stress for each of these nodes, with linear elements, versus the number of elements was plotted in Figure 4.3, and the values for the quadratic mesh are plotted in Annex A. The values were obtained for meshes with global seeds of 0.5, 0.2, 0.1, 0.05 and 0.02.

After the convergence study, the size of the global seeds was chosen for all the further computations, as well as the type of elements, shown in Table 4.1. The number of elements for each part was also depicted. In Figure 4.2 the final mesh for the complete eye is shown.

Table 4.1. Element type, global seeds size and number of elements for each part of the models.

	Elements Type	Global Seeds Size	Number of Elements
Cortex	CAX4	0.05	4644
Nucleus	CAX4	0.05	2648
Capsular Bag	MAX1	0.05	200
Zonules	MAX1	0.05	44
IOL	CAX4R/CAX3	0.05	1338

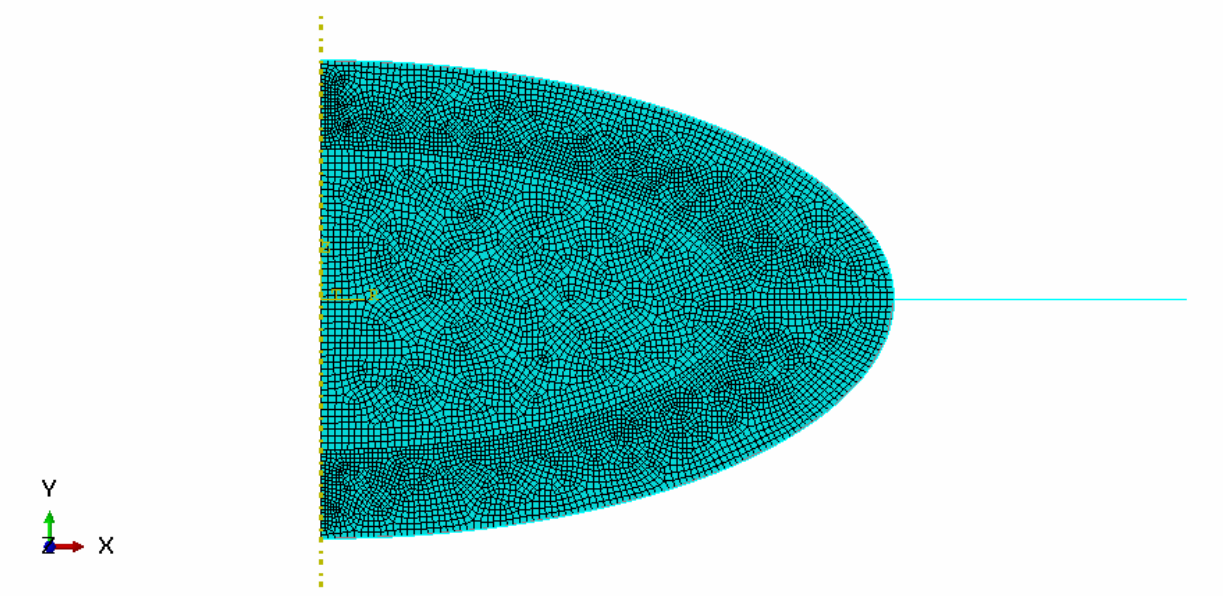

Figure 4.2. Final mesh for each part of the model, with global seeds with a size of 0.05.

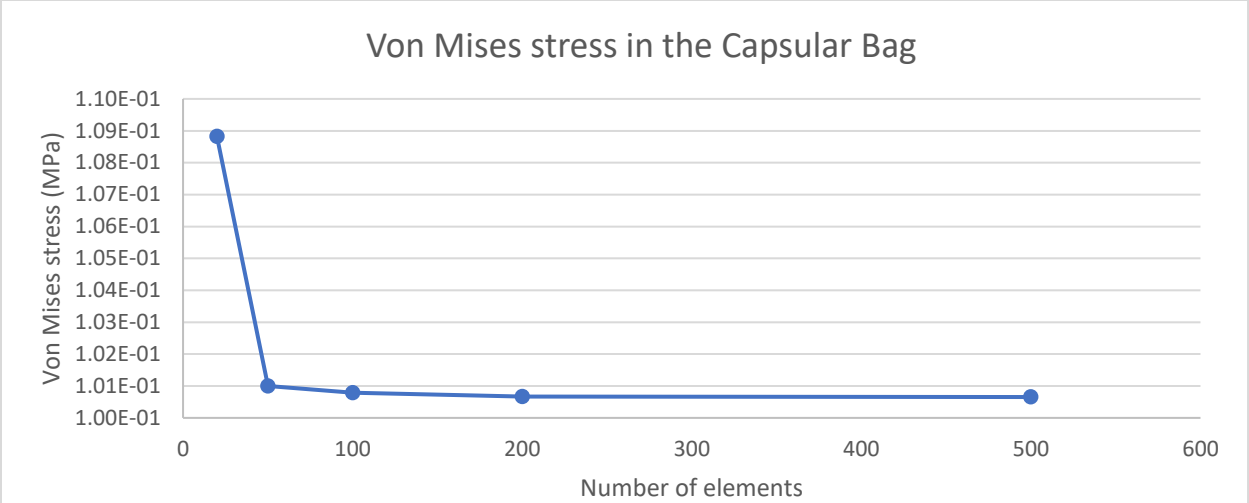

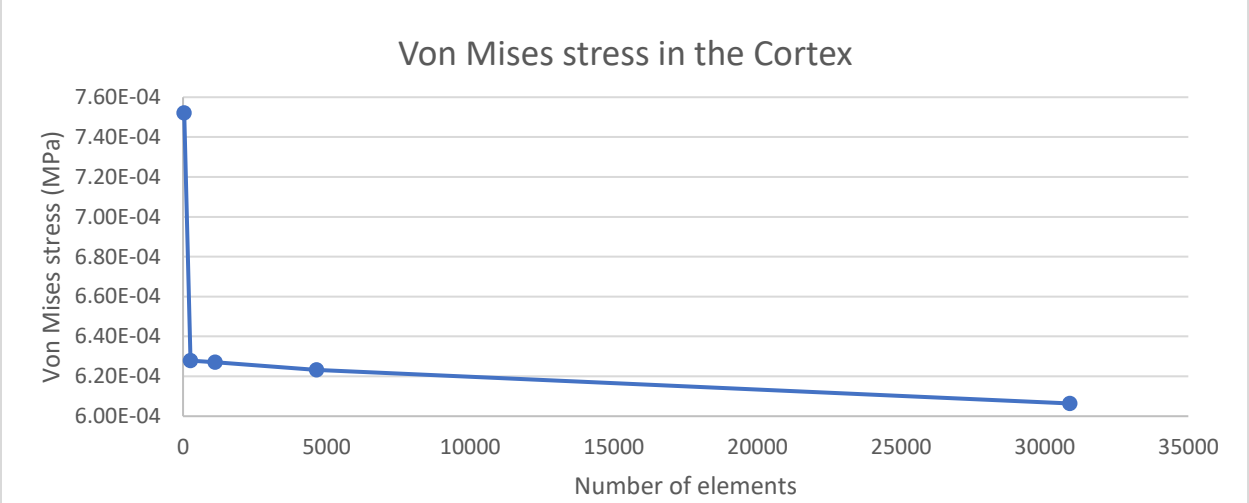

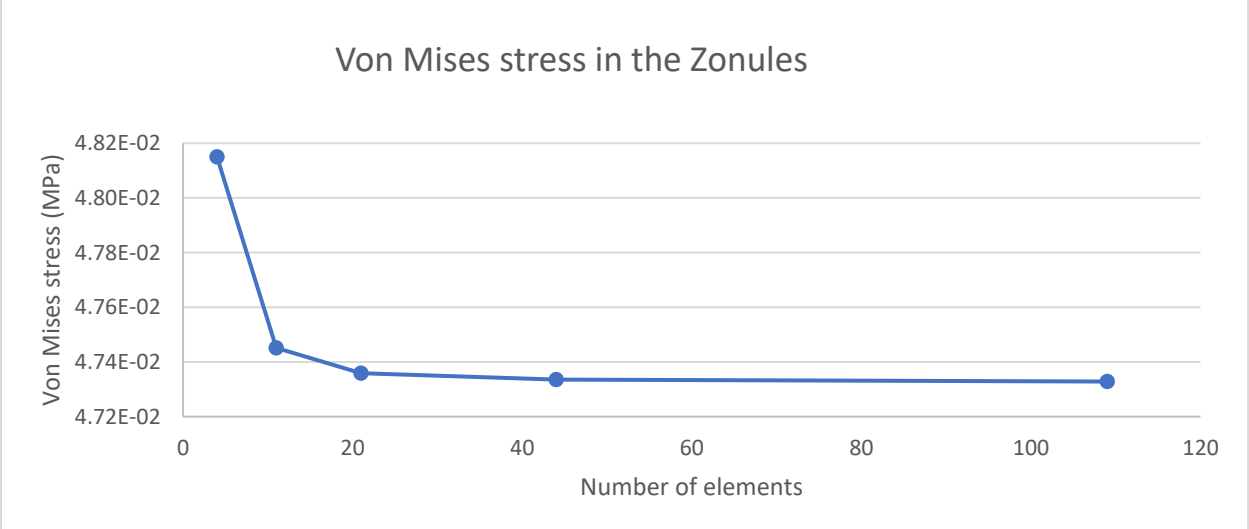

Figure 4.3. Values of the von Mises stress (MPa) for the nodes in the capsular bag, cortex and zonules, used in the convergence study versus the number of elements for each parts.

4.2. Numerical/Experimental Comparison

Figure 4.4 displays the superposition of the accommodated and the unaccommodated eye with a membrane elements capsular bag and let us compare the change in length in radial direction (δ_R) and in total lens thickness (δ_T), i.e., in the X and in the Y direction respectively. The lens had an increase of about 0.35 mm in the radial direction, corresponding to approximatively 8% of its initial diameter, very close to the change of 7% stated by Weeber & van der Heijde (2008), and a decrease of 0.25 mm in lens thickness. This value of δ_R was higher than the one found by Burd et al. (2002) of 0.290 mm but was very close to the one found by Lanchares et al. (2012) of 0.32 mm. Regarding the lens thickness δ_T, Dubbelman et al. (2003) and Lanchares et al. had output values of 0.33 mm and 0.39 mm respectively, values that were higher than the one measured in this study. In

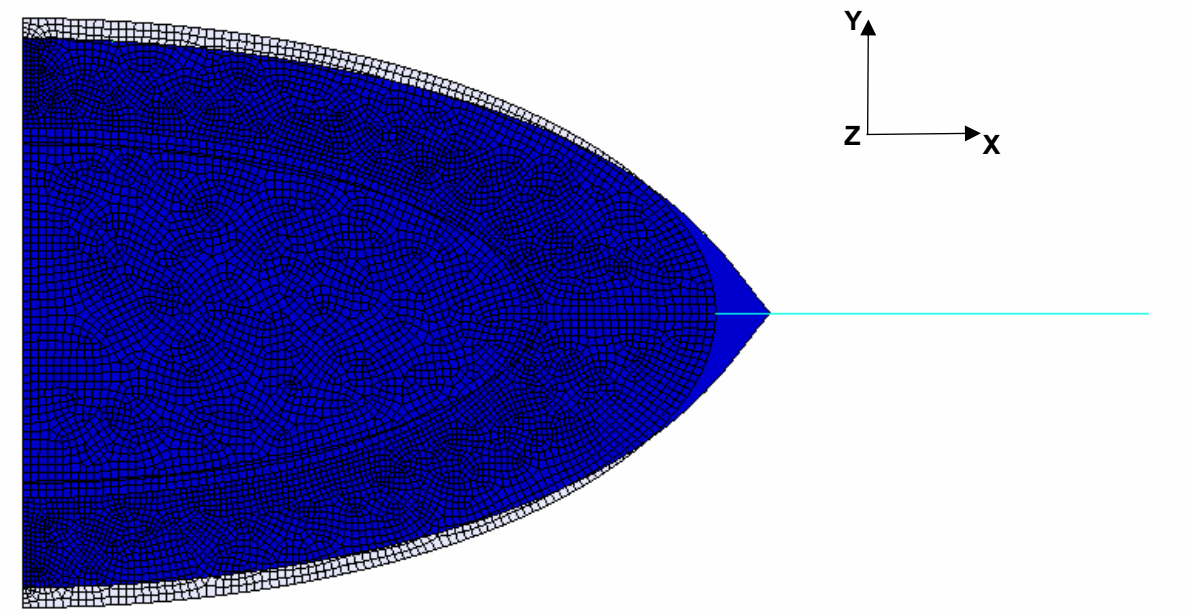

Figure 4.4. Accommodated (meshed) and disaccommodated (unmeshed) eye model with the membrane elements capsular bag. A decrease in lens thickness (in Y direction) and an increase in radial thickness (X direction) is noticeable.

Table 4.2 a summary of changes in axial and radial lengths is shown.

Table 4.2. Summary of changes in axial and radial lengths in mm and in percentage. The initial radius of the lens (R_{lens}) as well as its initial thickness (T_{lens}) are shown.

	R_{lens} (mm)	T_{lens} (mm)	δ_R (mm)	δ_R (%)	δ_T (mm)	δ_T (%)
Membrane Capsule	4.30	3.60	0.35	8.1	0.25	6.9
Shell Capsule	4.30	3.60	0.35	8.1	0.25	6.9
Dubbelman et al., 2003	-	3.63	-	-	0.33	9.1
Lanchares et al., 2012	4.88	3.57	0.32	6.6	0.39	10.9
Burd et al., 2002	3.83	-	0.29	7.6	-	-

The maximum principal stress distribution shown in Figure 4.5 (A), representing the capsular bag in the unaccommodated state, shows a range of stresses going from 6.9×10^{-2} to 1.6×10^{-1} MPa, that were of the same order than the ones from Lanchares et al., that went from 5.3×10^{-2} to 1.6×10^{-1} MPa. The distribution of stress was slightly different, since Lanchares et al. used a variable thickness of the capsule, with the maximum value corresponding to the posterior pole associated with the thinner thickness. Taking the maximum logarithmic strain of the capsular bag, in Figure 4.5 (B), equal to 0.0738, it was easy to compute the strain $\lambda_{principal} = e^{LE} = e^{0.0738} = 1.0766$, i.e., 7.66%. This value was very similar to the 7.28% strain computed by Lanchares et al. Another parameter that could be compared with the literature, was the resulting force in the zonules after their displacement. The resulting force computed at the tip of the zonules had a magnitude of 0.071 N, that was in the same range as the 0.078 N from Lanchares et al. and the 0.08-0.1 N from Burd et al. (2002).

In the first step of this work, comparing with other studies, this model was considered acceptable despite the simplification made during its construction, such as its geometry and the constant thickness of the capsule. To understand the influence of shell elements or membrane elements in the capsular bag, a comparison of the von Mises stresses in the capsule and nucleus-cortex was made.

Even though the local maximum von Mises stress in the capsular bag was different in both models, the stress distribution remained the same, as shown in Figure 4.6 (A)(B). In the capsule with shell elements, the maximum was almost two times higher than in the model with membrane elements, in the area where it was being pulled by the zonules.

It was also important to understand if a different capsular bag could have an influence in the inner part of the crystalline, i.e., in the nucleus and the cortex. As shown in Figure 4.6 (C)(D), the distribution of stresses was almost the same, with once again only a difference in the local maximums, letting us conclude that the model with a shell elements capsular bag was very similar to the one with membrane elements and could be acceptable to further study the cataract surgery

In both models, the stress in the zonules was almost constant, standing in the range of 4.7×10^{-2} MPa, for the membrane and shell capsule.

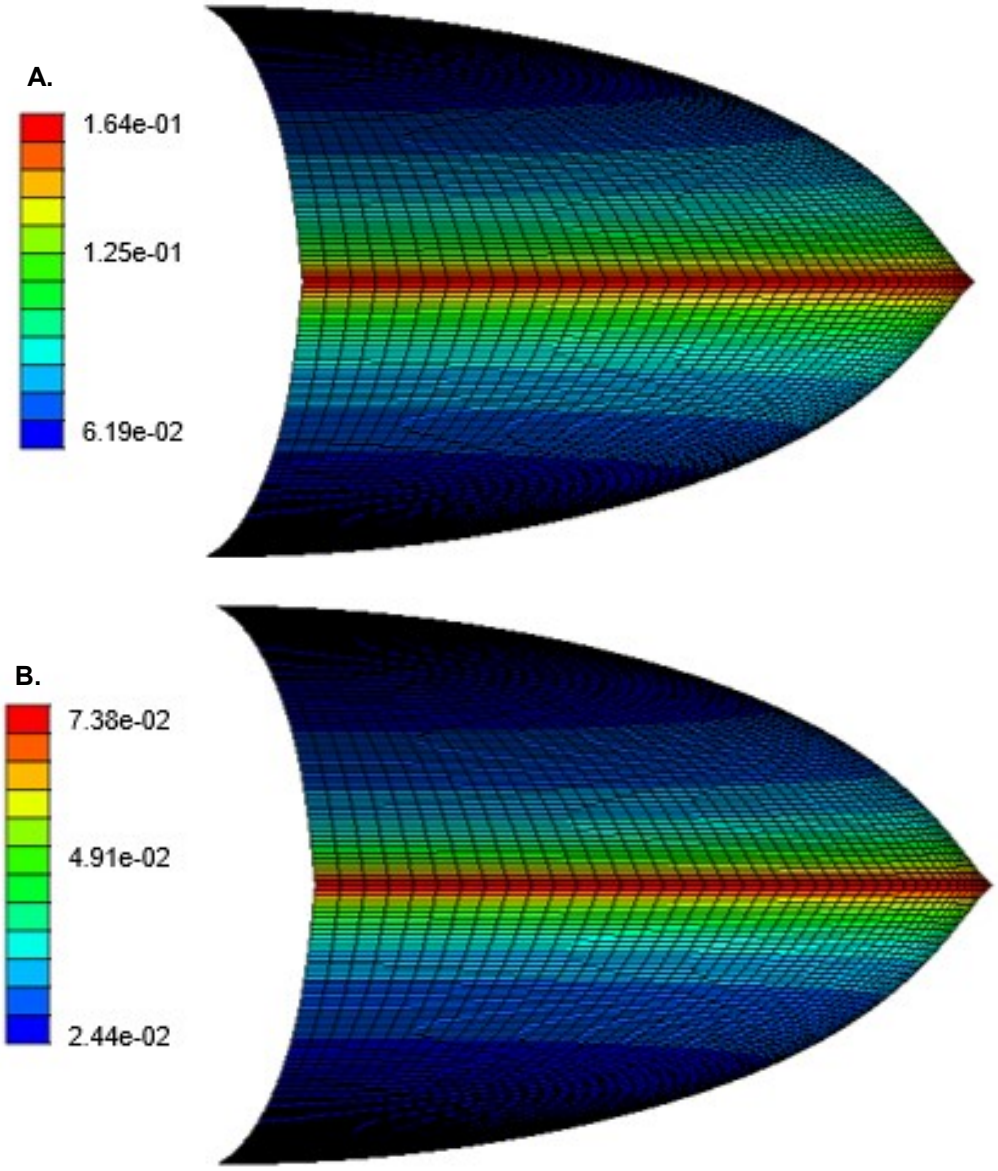

Figure 4.5. (A) Maximum principal stress in the membrane elements capsule in the fully unaccommodated state in MPa, (B) Maximum principal in-plane logarithmic strain in the membrane elements capsule in the fully unaccommodated state. Both figures are obtained after revolving the capsular bag around the axis of symmetry, giving a three-dimensional aspect to the axisymmetric model.

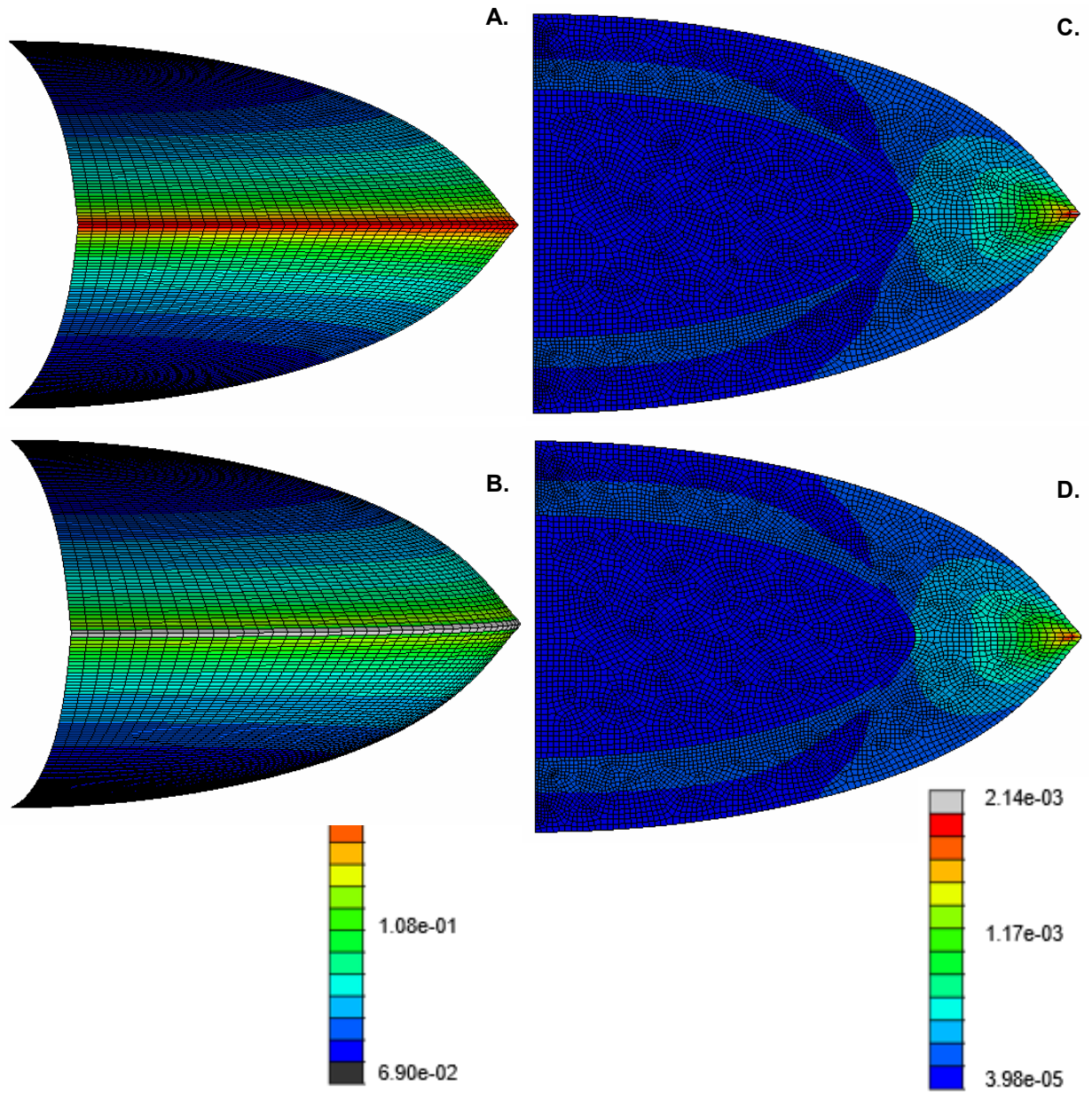

Figure 4.6. Von Mises stresses (MPa) in the capsular bag, following disaccommodation: (A) Membrane elements capsular bag, (B) Shell elements capsular bag; Von Mises stresses (MPa) in the cortex and nucleus of the crystalline, following disaccommodation: (C) Model with membrane elements capsular bag, (D) Model with shell elements capsular bag. Figures A and B are obtained after revolving the capsular bag around the axis of symmetry, giving a three-dimensional aspect to the axisymmetric model.

5. Results

In this chapter, the outcomes of the simulations after the validation of the model will be presented and compared. For each model, the von Mises stress in the zonules (S_Z), in the capsular bag (S_{CB}) and in the IOL (S_{IOL}), were assessed, as well as the radial displacement (δ_r) and the resulting force at the tip of the zonules (RF_Z). All the models built had the purpose to let us compare different models for pseudophakic eyes, with different diameters of capsulorhexis, different materials for the one-piece IOLs and with different traction forces towards the center of the capsulorhexis, that simulated part of the process of fibrosis.

All the computed results that did not appear in this section were depicted in Annex B.

5.1. Post-Surgery

A comparison between the eye before (model *M1*) and after surgery with a small capsulorhexis, a hydrophilic acrylic IOL and no traction force (model *M 2.1*) was possible. The values of stresses, radial displacement and resulting force are shown in Table 5.1 for both models. The values of stresses in the zonular fibers is almost the double from *M1* to *M 2.1*, going from an average value of 4.7×10^{-2} MPa to 8.9×10^{-2} MPa, and from the crystalline to the IOL it substantially increased 30 times from an average value of 1.9×10^{-4} MPa to 5.8×10^{-3} MPa, whereas in the capsular bag the values decreased, going from average values of 8.0×10^{-2} MPa to 1.9×10^{-3} MPa. The radial displacement in *M 2.1*, equal to 7.3×10^{-3} mm was almost fifty times smaller than in *M1*, 3.5×10^{-1} mm. Another value that increased from *M1* to *M 2.1* was the resulting force at the tip of the zonular fibers, with computed values of 7.1×10^{-2} N and 12.8×10^{-2} N for the model before and after surgery, respectively. All these outcomes were expected with the increase of stiffness of the three IOL materials in comparison with the natural cortex and nucleus of the crystalline.

Table 5.1. Minimum and maximum values of von Mises stresses in the zonular fibers, capsular bag and crystalline/IOL, as well as radial displacement and resulting force at the tip of the zonular fibers for the models M1 and M 2.1.

Model	Variables	Range	Average Value
M1	S_Z (MPa)	$4.7 \times 10^{-2} – 4.7 \times 10^{-2}$	4.7×10^{-2}
	S_{CB} (MPa)	$6.9 \times 10^{-2} – 1.5 \times 10^{-1}$	8.0×10^{-2}
	S_{IOL} (MPa)	$4.0 \times 10^{-5} – 2.1 \times 10^{-3}$	1.9×10^{-4}
	δ_r (mm)	3.5×10^{-1}	-
	RF_Z (N)	7.1×10^{-2}	-
M 2.1	S_Z (MPa)	$8.4 \times 10^{-2} – 9.7 \times 10^{-2}$	8.9×10^{-2}
	S_{CB} (MPa)	$3.3 \times 10^{-4} – 3.7 \times 10^{-2}$	1.9×10^{-3}
	S_{IOL} (MPa)	$3.0 \times 10^{-3} – 4.4 \times 10^{-2}$	5.8×10^{-3}
	δ_r (mm)	7.3×10^{-3}	-
	RF_Z (N)	12.8×10^{-2}	-

With a maximum of 1.5 x 10^{-1} MPa, the higher stress in *M1* was located on the capsular bag, whereas in model *M 2.1.* it was located on the zonular fibers with a value of 9.7 x 10^{-2} MPa.

5.2. Influence of the Stiffness of the IOL

To study the influence of the stiffness of the IOL in the pseudophakic eye, a comparison between models *M 2.1.*, *M 2.2.* and *M 2.3.* was performed. These three models had the same Φ_{ccc} and TF, equal to zero, but differed in their IOL material and consequently, in their stiffness. The results drawn in this section can be drawn for every other three sets of models, that only differ in IOL's stiffness.

Since the PMMA lens was at least 500 time stiffer than both acrylic lenses, the expected outcome would be that it would support more stress in it with a consequent decrease of stress in the capsular bag. This phenomenon is visible in Figure 5.1, where model *M 2.3.* had a different stress distribution, with the stress more distributed through the IOL haptic, than *M 2.1.* and *M 2.2.*, with a maximum value of 4.4 x 10^{-2} MPa, at the intersection between the capsular bag, the IOL and the insertion of the zonule. Whereas the general decrease of stress in the capsular bag was very slight between the hydrophilic and the hydrophobic acrylic lens, with average values going from 1.9 x 10^{-3} MPa to 1.4 x 10^{-3} MPa respectively, an accentuated change was clearly seen in model *M 2.3.*, with an average value of 8.9 x 10^{-6} MPa being 150 times lower than in *M 2.1.* and *M 2.2.* With the increase of stiffness of the IOL, a slight increase of the von Mises stress on the zonules was also noticeable, in the order of 1%, as well as a slight increase of the resulting force in the zonules, in the same order. With the increase of stiffness in the IOL, more resistance to the equatorial pull in the zonules in the materials would be encountered, leading to a big decrease of radial displacement in the IOL, with the one in model *M 2.3.,* 1.2 x 10^{-5} mm, being 6000 times higher than in the other two models, 7.3 x 10^{-3} mm for the hydrophilic and 5.0 x 10^{-3} mm for the hydrophobic acrylic lens.

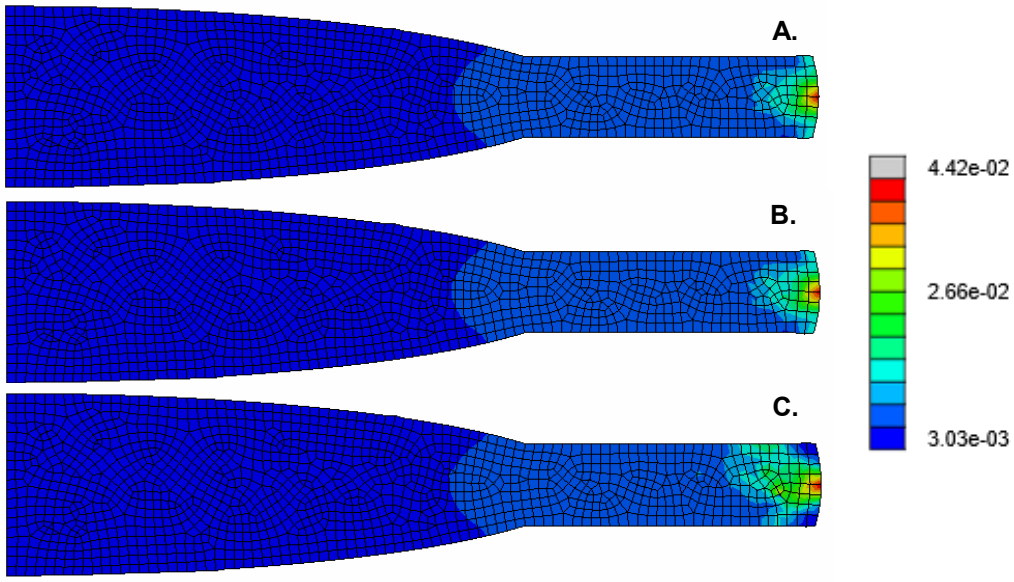

Figure 5.1. Von Mises stresses (in MPa) in the IOL, for the three models, after cataract surgery with a 4 mm CCC and no traction force, following ciliary body relaxation: (A) model M 2.1., (B) model M 2.2., (C) model M 2.3..

In Table 5.2, all the values for the outcomes are shown, and the values with the biggest changes noticeable are highlighted.

Table 5.2. Minimum and maximum values of von Mises stresses in the zonular fibers, capsular bag and IOL, as well as radial displacement and resulting force at the tip of the zonular fibers for the models M 2.1., M 2.2. and M 2.3.

Model	Variables	Range	Average Value
M 2.1.	S_Z (MPa)	$8.4 \times 10^{-2} – 9.7 \times 10^{-2}$	8.9×10^{-2}
	S_{CB} (MPa)	**$3.3 \times 10^{-4} – 3.7 \times 10^{-2}$**	**1.9×10^{-3}**
	S_{IOL} (MPa)	$3.0 \times 10^{-3} – 4.4 \times 10^{-2}$	5.8×10^{-3}
	δ_r (mm)	**7.3×10^{-3}**	-
	RF_Z (N)	12.8×10^{-2}	-
M 2.2.	S_Z (MPa)	$8.5 \times 10^{-2} – 9.8 \times 10^{-2}$	8.9×10^{-2}
	S_{CB} (MPa)	**$2.1 \times 10^{-5} – 3.3 \times 10^{-2}$**	**1.4×10^{-3}**
	S_{IOL} (MPa)	$3.1 \times 10^{-3} – 4.3 \times 10^{-2}$	5.9×10^{-3}
	δ_r (mm)	**5.0×10^{-3}**	-
	RF_Z (N)	12.9×10^{-2}	-
M 2.3.	S_Z (MPa)	$8.5 \times 10^{-2} – 9.9 \times 10^{-2}$	9.0×10^{-2}
	S_{CB} (MPa)	**$3.5 \times 10^{-9} – 2.6 \times 10^{-4}$**	**8.9×10^{-6}**
	S_{IOL} (MPa)	$4.0 \times 10^{-3} – 4.4 \times 10^{-2}$	6.1×10^{-3}
	δ_r (mm)	**1.2×10^{-5}**	-
	RF_Z (N)	12.9×10^{-2}	-

For these three models, the maximum values of stresses were in the zonules, with values of 9.7×10^{-2}, 9.8×10^{-2} and 9.9×10^{-2} MPa for the hydrophilic, hydrophobic acrylic and PMMA IOL, respectively.

5.3. Influence of the Traction Force

To study the influence of the traction force on the capsulorhexis on the pseudophakic eyes, models *M 2.1.*, *M 4.1.*, *M 6.1.* and *M 8.1.* were compared. They all had a one-piece IOL made of hydrophilic acrylic and the same Φ_{ccc} but differed in the traction force that was applied. It increased from 0 N to 0.15 N, from model *M 2.1.* to model *M 8.1.* The outcomes for this parametric study are depicted in Table 5.3.

With the increase of the traction force, no change in stress in the zonules nor in the resulting force at their tip was noticeable, with an average value of 8.9×10^{-2} MPa for the stress and 12.9×10^{-2} N for the resulting force in all models. The stress in the capsular bag, had a slight decrease of maximum values 3.72×10^{-2} MPa in the first model and 3.31×10^{-2} MPa in the last. But overall, the average value of stress in the capsular bag increased 3.5 times from the model with no traction force to the one with a traction force of 0.15 N. The stress in the IOL and radial displacement had the greatest change, with the maximum stress, of 1.5×10^{-1} MPa, in the IOL of *M 8.1.* being more than three times the maximum stress, equal to 4.4×10^{-2} MPa, in *M*

2.1. The radial displacement, 7.3 x 10^{-3} mm, in *M 2.1.* was almost three times higher than the one in *M 8.1.*, 2.8 x 10^{-3} mm.

Table 5.3. Minimum and maximum values of von Mises stresses in the zonular fibers, capsular bag and IOL, as well as radial displacement and resulting force at the tip of the zonular fibers for the models M 2.1., M 4.1., M 6.1. and M 8.1.

Model	Variables	Range	Average Value
M 2.1.	S_Z (MPa)	8.4 x 10^{-2} – 9.7 x 10^{-2}	8.9 x 10^{-2}
	S_{CB} (MPa)	3.3 x 10^{-4} – 3.7 x 10^{-2}	1.9 x 10^{-3}
	S_{IOL} (MPa)	3.0 x 10^{-3} – 4.4 x 10^{-2}	5.8 x 10^{-3}
	δ_r (mm)	7.3 x 10^{-3}	-
	RF_Z (N)	12.8 x 10^{-2}	-
M 4.1.	S_Z (MPa)	8.5 x 10^{-2} – 9.8 x 10^{-2}	8.9 x 10^{-2}
	S_{CB} (MPa)	1.5 x 10^{-3} – 2.6 x 10^{-2}	4.0 x 10^{-3}
	S_{IOL} (MPa)	6.0 x 10^{-4} – 6.8 x 10^{-2}	7.7 x 10^{-3}
	δ_r (mm)	4.2 x 10^{-3}	-
	RF_Z (N)	12.9 x 10^{-2}	-
M 6.1.	S_Z (MPa)	8.5 x 10^{-2} – 9.8 x 10^{-2}	8.9 x 10^{-2}
	S_{CB} (MPa)	1.6 x 10^{-3} – 4.6 x 10^{-2}	6.0 x 10^{-3}
	S_{IOL} (MPa)	9.5 x 10^{-4} – 1.3 x 10^{-1}	1.2 x 10^{-2}
	δ_r (mm)	3.2 x 10^{-3}	-
	RF_Z (N)	12.9 x 10^{-2}	-
M 8.1.	S_Z (MPa)	8.5 x 10^{-2} – 9.8 x 10^{-2}	8.9 x 10^{-2}
	S_{CB} (MPa)	1.8 x 10^{-3} – 3.3 x 10^{-2}	6.7 x 10^{-3}
	S_{IOL} (MPa)	1.2 x 10^{-3} – 1.5 x 10^{-1}	1.4 x 10^{-2}
	δ_r (mm)	2.8 x 10^{-3}	-
	RF_Z (N)	12.9 x 10^{-2}	-

It was also interesting to observe a change of maximum stress in all the model, i.e., for the models with traction forces below RF_X the local maximum stress was located in the zonules, whereas for the models with traction forces greater than this value it was located in the IOL, at the contact point with the edge of the capsulorhexis. These local maximums are highlighted in Figure 5.2. The only exceptions were models *M 7.1.*, *M 7.2.*, *M 9.1.* and *M 9.2.* where the local maximum was in the capsular bag, at the edge of the CCC.

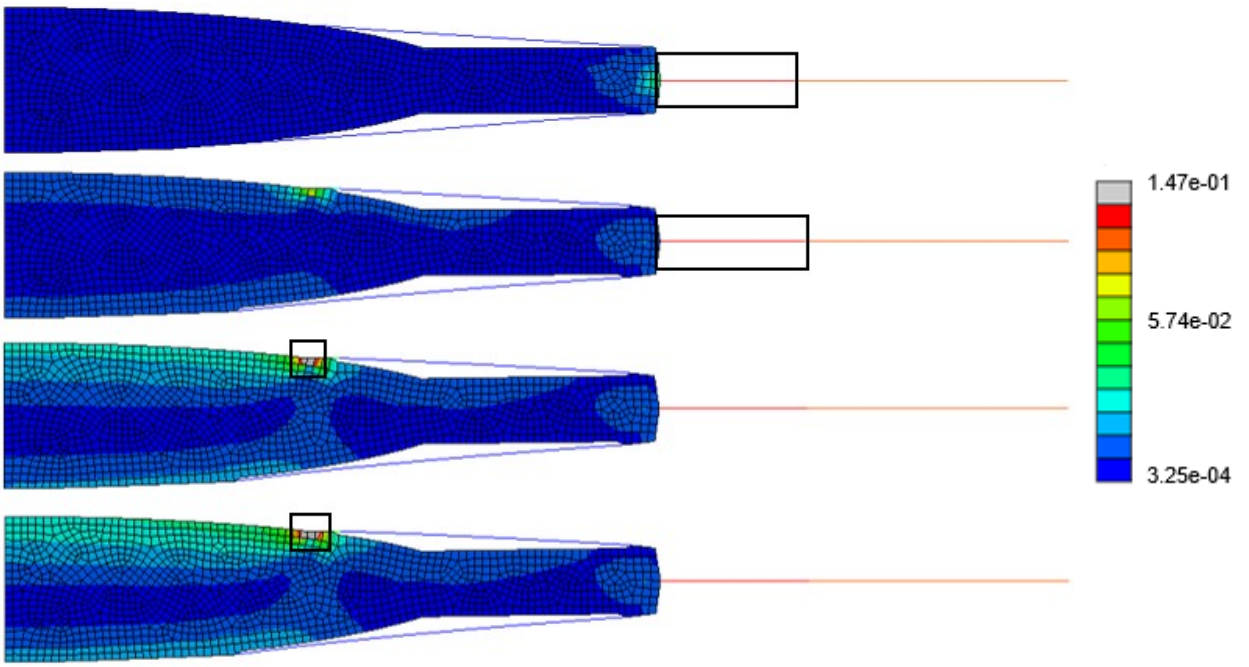

Figure 5.2. Von Mises stresses in all the components of the four models, after cataract surgery with a 4 mm CCC and a hydrophilic acrylic IOL, following ciliary body relaxation: (A) model M 2.1., (B) model M 4.1., (C) model M 6.1. and (D) model M 8.1. The local maximum stresses are highlighted in the black boxes.

5.4. Influence of the Diameter of the Capsulorhexis

In this subsection, models *M 2.1.* and *M 3.1.* will be compared, as well as models *M 4.1.* and *M 5.1*. The first two had the same IOL material (hydrophilic acrylic) and the same traction force equal to zero but differed in the size of the capsulorhexis. The other two models had the same material properties but had a traction force applied at the opening of the capsulorhexis of 0.07 N. Models *M 2.1.* and *M 4.1.* had a small capsulorhexis with a 4 mm diameter and models *M 3.1.* and *M 5.1.* had a large one, with a 4.5 mm diameter.

With no traction force applied, the distributions and values of stress in the zonules were the same in both models, with average values of 8.9 x 10^{-2} MPa. For the stress in the capsular bag and in the IOL, the maximum values of stress remained the same with the increase of diameter of the capsulorhexis, with the average value of stress in the capsule increasing slightly in the order of 16%, whereas the average value of stress in the IOL remained the same. The radial displacement was almost the same, with 7.3 x 10^{-3} mm and 7.2 x 10^{-3} mm, for *M 2.1.* and *M 3.1.*, respectively, with only a variance in the order of 1%. The resulting force in both models were also very similar, with a variance of 0.7%, that could be neglected. All the results for both models are shown in Table 5.4.

In this subsection, there was a need to perform another outcomes analysis, since with traction force in the opening of the capsulorhexis, the values between the same models with different Φ_{ccc} changed more than with no traction force.

Table 5.4. Minimum and maximum values of von Mises stresses in the zonular fibers, capsular bag and IOL, as well as radial displacement and resulting force at the tip of the zonular fibers for the models M 2.1. and M 3.1.

Model	Variables	Range	Average Value
M 2.1.	S_Z (MPa)	$8.4 \times 10^{-2} – 9.7 \times 10^{-2}$	8.9×10^{-2}
	S_{CB} (MPa)	$3.3 \times 10^{-4} – 3.7 \times 10^{-2}$	1.9×10^{-3}
	S_{IOL} (MPa)	$3.0 \times 10^{-3} – 4.4 \times 10^{-2}$	5.8×10^{-3}
	δ_r (mm)	7.3×10^{-3}	-
	RF_Z (N)	12.8×10^{-2}	-
M 3.1.	S_Z (MPa)	$8.4 \times 10^{-2} – 9.7 \times 10^{-2}$	8.9×10^{-2}
	S_{CB} (MPa)	$4.3 \times 10^{-4} – 3.7 \times 10^{-2}$	2.2×10^{-3}
	S_{IOL} (MPa)	$4.1 \times 10^{-3} – 4.4 \times 10^{-2}$	5.8×10^{-3}
	δ_r (mm)	7.2×10^{-3}	-
	RF_Z (N)	12.9×10^{-2}	-

The stress in the zonules was still the same, with an average value of 8.9×10^{-2} MPa for both models. The values are all displayed in Table 5.5. The average and maximum value of stress in the IOL decreased with the increase of the diameter of the capsulorhexis, with average values of 7.7×10^{-3} MPa and of 7.4×10^{-2} MPa and maximum values of 6.8×10^{-2} MPa and 5.2×10^{-2} MPa, for models *M 4.1.* and *M 5.1.*, respectively. The decrease in average values of stress was in the order of the 4%, whereas in the maximum stress it was 31%. The stresses in the IOL are shown in Figure 5.3, where even though model *M 4.1.* has a higher local stress in the point where the traction force is applied, model *M 5.1.* showed higher values of stress in the haptic, near the insertion point of the zonule. In the capsular bag, the maximum stress value computed for model *M 5.1.,* 7.8×10^{-2} MPa, was three times higher than the one computed for model *M 4.1.*, 2.6×10^{-2} MPa, but had slight increase of 5% of average values from the model with the smaller CCC to the one with the larger CCC. Whereas the resulting force at the tip of the zonules remained constant with a value of 12.9×10^{-2} N, the radial displacement was almost 1.5 times higher in model *M 5.1.* than in model *M 4.1.*, with values of 5.9×10^{-3} mm to 4.2×10^{-3} mm, respectively.

Table 5.5. Minimum and maximum values of von Mises stresses in the zonular fibers, capsular bag and IOL, as well as radial displacement and resulting force at the tip of the zonular fibers for the models M 4.1. and M 5.1.

Model	Variables	Range	Average Value
M 4.1.	S_Z (MPa)	$8.5 \times 10^{-2} – 9.8 \times 10^{-2}$	8.9×10^{-2}
	S_{CB} (MPa)	$1.5 \times 10^{-3} – 2.6 \times 10^{-2}$	4.0×10^{-3}
	S_{IOL} (MPa)	$6.0 \times 10^{-4} – 6.8 \times 10^{-2}$	7.7×10^{-3}
	δ_r (mm)	4.2×10^{-3}	-
	RF_Z (N)	12.9×10^{-2}	-
M 5.1.	S_Z (MPa)	$8.4 \times 10^{-2} – 9.8 \times 10^{-2}$	8.9×10^{-2}
	S_{CB} (MPa)	$1.0 \times 10^{-3} – 7.8 \times 10^{-2}$	4.2×10^{-3}
	S_{IOL} (MPa)	$5.2 \times 10^{-4} – 5.2 \times 10^{-2}$	7.4×10^{-3}
	δ_r (mm)	5.9×10^{-3}	-
	RF_Z (N)	12.9×10^{-2}	-

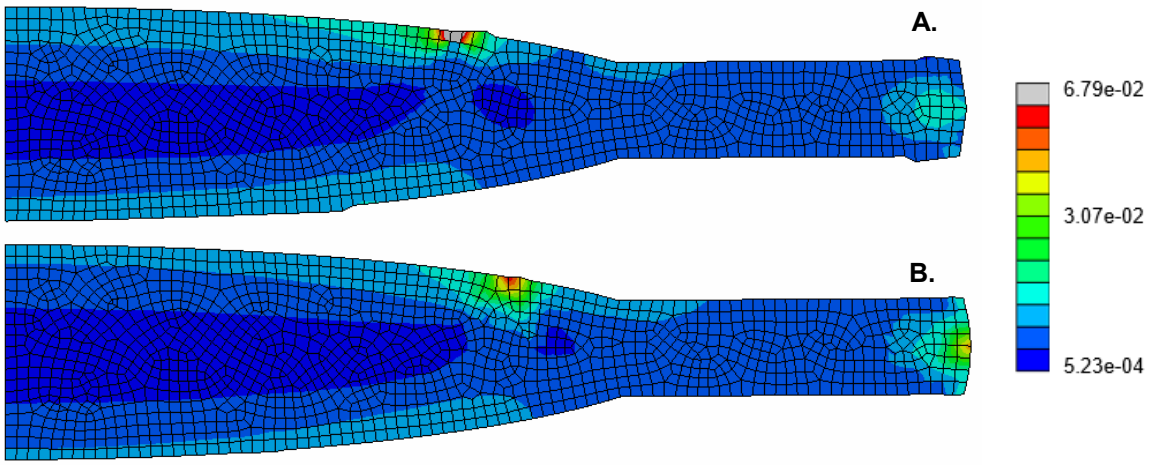

Figure 5.3. Von Mises stresses in the hydrophilic acrylic IOL (in MPa), for the two models, after cataract surgery and a traction force of 0.07N, following ciliary body relaxation: (A) model M 4.1., (B) model M 5.1.

5.5. Maximum stress

Another important aspect to assess was the maximum values of stress in each of the models. For all the models, when the traction force was lower than their respective RF_X, the maximum stress was in the zonules, near their insertion point in the capsular bag (Figure 5.4). For all the models with small capsulorhexis and the models with PMMA material and a large capsulorhexis, when the traction force became equal or higher than RF_X, the maximum value of stress laid in the IOL near the node where the traction force was applied (Figure 5.4 and Figure 5.6). For the models with large capsulorhexis, made of hydrophilic or hydrophobic acrylic and with a traction force equal or higher than RF_X, the maximum stress was in the capsular bag (Figure 5.5). The dashed line in the figures represents the value of RF_X.

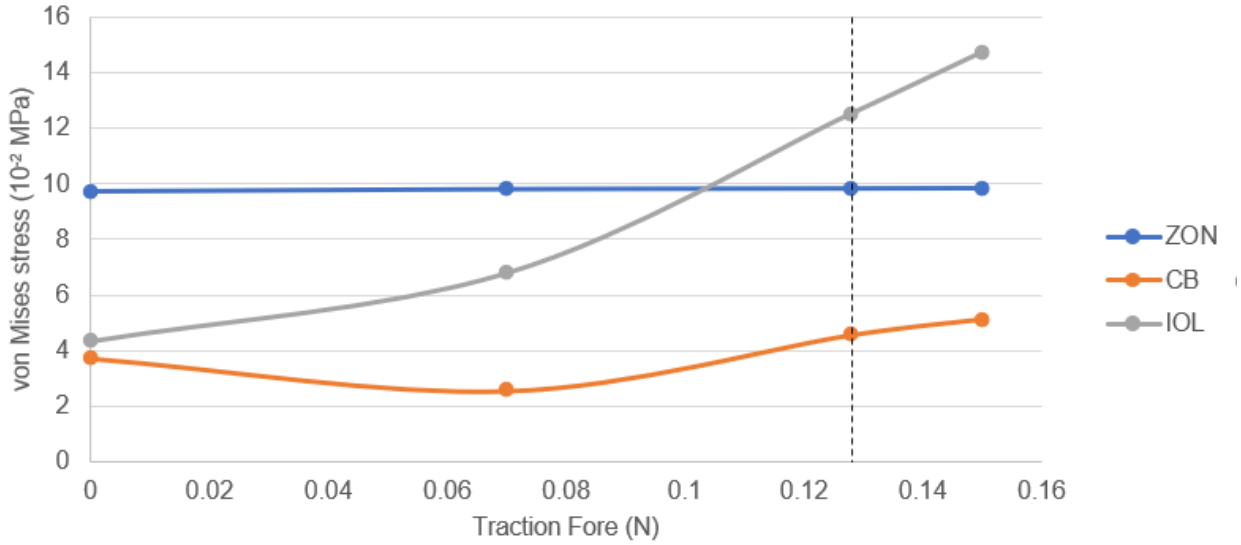

Figure 5.4. Maximum von Mises stress in the zonules, the capsular bag and the IOL (in 10^{-2} MPa) versus the traction force (in N) applied at the opening of the capsulorhexis, for the hydrophilic acrylic IOL model with a 4 mm CCC.

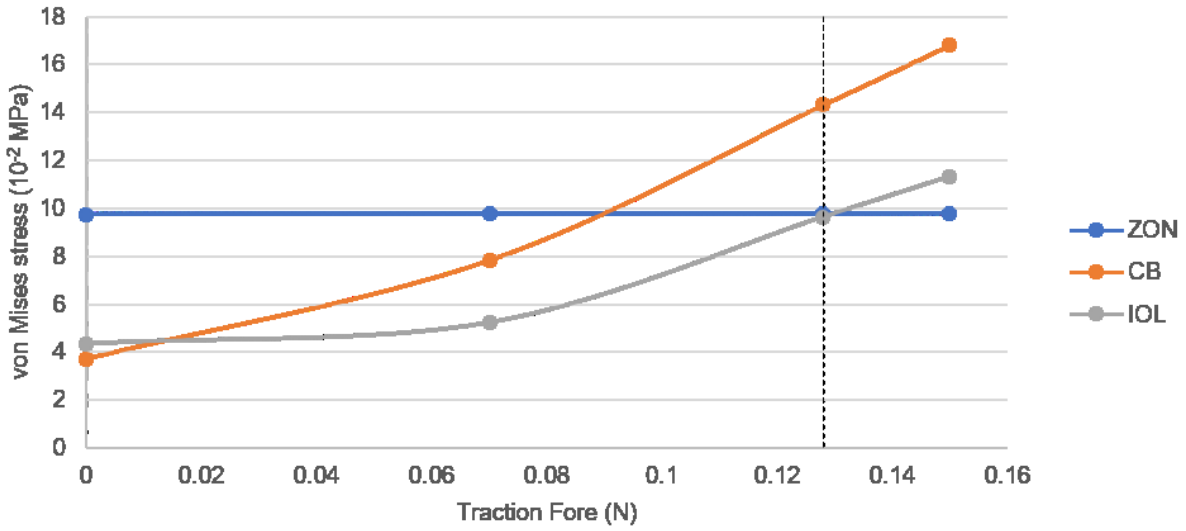

Figure 5.5. Maximum von Mises stress in the zonules, the capsular bag and the IOL (in 10^{-2} MPa) versus the traction force (in N) applied at the opening of the capsulorhexis, for the hydrophilic acrylic IOL model with a 4.5 mm CCC.

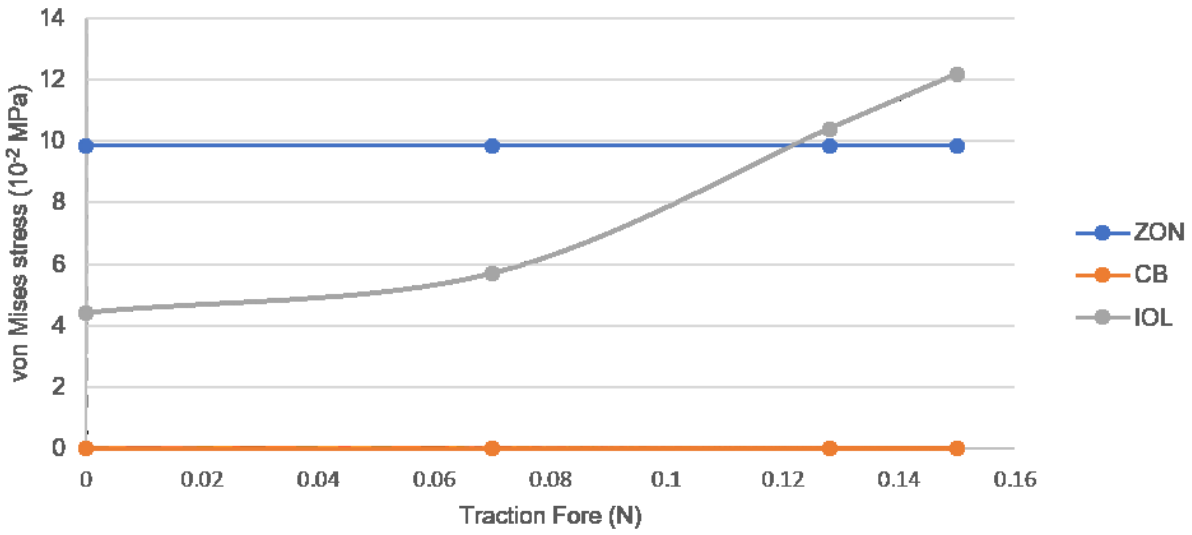

Figure 5.6. Maximum von Mises stress in the zonules, the capsular bag and the IOL (in 10^{-2} MPa) versus the traction force (in N) applied at the opening of the capsulorhexis, for the PMMA IOL model with a 4.5 mm CCC.

5.6. Summary

All parameters tested showed they had some influence on the overall model. In summary, with the increase of the traction force and of the stiffness of the materials, i.e., their Young's modulus, the stress in the zonules and in the IOL would increase, as well as the resulting force at the tip of the zonules, whereas the stress in the capsular bag and the radial displacement would decrease. With the increase of the diameter of the capsulorhexis, and the traction force equal to zero, the overall stress in the models would not change, while the radial displacement would decrease and the resulting force increase, but so very slightly they were not considered as significant. Finally, with the increase of the diameter of the capsulorhexis, with the traction force greater than zero, all the parameters studied would have a contrary behavior than the ones described earlier, i.e., the stress in the zonules and in the IOL decreased, as well as the resulting force at the tip of the zonules, whereas the stress in the capsular bag and the radial displacement increased. This summary is depicted in Table 5.6.

Table 5.6. Summary of the variation of the average values of stress in the zonules, the capsular bag and in the IOL, as well as the radial displacement and resulting force at the tip of the zonules in all the models, with the increase of the Young's modulus, the traction force and the diameter of the capsulorhexis. The up arrow (↑) represents the increase of a parameter whereas the down arrow (↓) represents the decrease.

	S_z	S_{CB}	S_{IOL}	δ_R	RF_Z
Young's modulus	-	↓	↑	↓	-
TF	-	↑	↑	↓	-
Φ_{CCC}, TF=0	-	↑	-	-	-
Φ_{CCC}, TF>0	-	↑	↓	↑	-

It was also important to notice that across all models of pseudophakic eyes, the part that would undergo less change were the zonules, where no parameter seemed to influence greatly their maximum and average values of stress nor the resulting forces computed at their tips. The maximum variation between the average values of stress was of 1% and between the resulting force was 0.8%.

6. Discussion and Conclusions

6.1. Discussion

The complete eye before surgery that was modelled by an axisymmetrical model in this work yielded very similar results compared to previous studies, of maximum and distribution of stresses, as well as of resulting forces in the zonules and displacement in the radial direction and in lens thickness. Even though simplifications were made in the properties of materials, i.e., considering all the materials as linearly elastic isotropic, and in the geometry of the crystalline, the presented model could be validated. It was also demonstrated that a model with a shell capsular bag instead of a membrane one yielded very similar outcomes and could also be used in the modulation of the crystalline under cataract surgery.

Comparing the human crystalline complex with a pseudophakic eye, a decrease of stress in the capsular bag and of radial displacement of the new complex was observed, with a consequent increase of resulting force and stress in the zonules, as well as an increase in stress in the IOL. These outcomes could be compared with the influence of the stiffness of the IOL material through the pseudophakic models, since the biggest difference in the eye after surgery, is the difference in stiffness of the human crystalline compared with the stiffness of all the synthetic IOL materials. The IOLs were at least a thousand times stiffer than any component of the crystalline, making them support more stress than the crystalline and consequently relieve the stress in the capsular bag. With all the models undergoing the same displacement of 0.5 mm at the tip of the zonules, the stiff IOLs lead to the zonules having to stretch more to pull the lens and the capsular bag, and consequently putting the zonular fibers in a higher state of stress, with its maximum at the intersection node of the three parts of the model. On one hand, the IOLs gave more support to minimize stress in the capsule and eventually decrease its risk of rupture, but on the other hand it put the zonules into a state of more stress with a higher possibility for them to break and lead to an IOL-capsular bag dislocation. Ideally, to avoid this post-operative complication, a lens with a stiffness closer to the one of the human crystalline would be the best solution to try and maintain the state of stress of the capsular bag and the zonules closer to their original state.

Comparing only pseudophakic eyes, knowing that the stiffer PMMA IOL was at least 500 times stiffer than the acrylic lenses, a slight increase of 5% in average stress of the IOL can be considered negligible. The biggest changes observed while increasing the stiffness of the IOLs was a big decrease in average capsular stress and in radial displacement. This outcome is comparable with the case studied before, i.e., the substitution of the crystalline with any IOL, where an increase in IOL stiffness would give more support to the capsular bag and minimize its average stress. In the zonules, no change in maximum and average values of stress was observed, nor change in the resulting force at their tip.

The increase of the traction force at the opening of the capsulorhexis showed a big influence in the distribution of stress in all the model, increasing the stress in the IOL (principally in its optic) and decreasing the radial displacement, substantially. Even without knowing the *in vivo* values of the traction force at the

edge of the capsulorhexis, it was relevant to study it to understand if the models built in this work were sensible to its variation. As it was shown previously, the stress in the IOL and the capsular bag (for acrylic lenses with a large capsulorhexis) were very sensible to this variation changing the maximum values of stress from the zonules to either the capsular bag or the IOL. It was expected to observe an increase in average stress in the capsular bag and in the IOL, since these two parts were subjected to an increasing load in the opposite direction from that of the ciliary body relaxation. Furthermore, Hudish et al. stated that with fibrosis on the edge of the capsulotomy, leading to ACCS, the apparition of a centripetal force towards the center of its opening, greater than the force exerted by the zonules, could lead to the rupture of the zonular fibers and cause late IOL-capsular bag dislocation (Hudish et al., 2017). But in this work, it was shown that an increase of this centripetal force, i.e., the traction force that was applied, did not influence the average stress in the zonules, even when it was higher than the resulting force in the zonules.

A small and large capsulorhexis, with 72.73% and 82.83% of the diameter of the IOL optic, with no traction force applied at the edge of the capsulorhexis were compared and did not seem to have a direct impact on the stresses in two parts of the model. Only the capsular bag seemed to have a slight increase of 16% in its average stress, with the increasing diameter of the CCC. Since it was known that the size of the capsulorhexis had an impact on some post-surgery complications (Langwińska-Wośko et al., 2011), the outcomes found did not seem realistic. That was why the decision to simulate the traction force at the edge of the capsulorhexis was made, even without knowing the *in vivo* values of this force. Even though the stress of all the parameters, the radial displacement and the resulting force seemed to be more sensible to changes in diameter than without traction force, the variation in the stress of the zonules was not considerable. With a larger capsulorhexis, it was shown that the distribution and values of stress in the haptic of the IOL and in the capsular bag were higher than with a small one. These results not only confirmed how important it was to model the traction forces, since they influenced all the parts the model, but lead us to understand that with a smaller capsulorhexis it was possible to relieve the stress in the capsular bag and eventually avoid its rupture, and a consequent IOL dislocation. This outcome seemed to be contrary to the one given by Gimbel et al. (2005) that stated that a smaller capsulorhexis lead to a higher probability of incidence of IOL-capsular bag dislocation, because it developed more ACCS than a large capsulorhexis. In this work, it was assumed that both large and small capsulorhexis had suffered ACCS and that the resulting traction force on its edge was the same in both cases. For that same traction force, the smaller capsulorhexis seemed more favorable in giving support to the capsular bag.

In summary, after surgery the stress in the zonules almost doubled in every model whereas in the capsular bag it decreased greatly in almost every model (except for models with hydrophilic or a hydrophobic acrylic lens, a large capsulorhexis and a traction force higher than their respective RF_X, i.e., *M17*, *M18*, *M23* and *M24*), due to the increased stiffness in any IOL compared with the crystalline. The fact that the IOLs had a stiffness at least a thousand times higher than the human crystalline lead to the IOLs giving a bigger support to the capsular bag, relieving it of stress. No parameter studied lowered the general state of stress in the zonules post-surgery. The simplified geometry of the natural human crystalline lens model, that could have

an impact on the distribution of stress in the capsular bag, did not seem to influence the outcomes of the pseudophakic eye models, since after surgery the capsule had a completely different shape, and shrank itself to the IOL.

6.2. Conclusions

Even though a few simplifications were made during the construction of the complete crystalline, such as a simplified geometry with a perfect ellipsoid shape for the crystalline lens and linear isotropic materials, the models with a membrane capsular bag and a shell capsular bag could both be compared with previous numerical models and proved to be capable of replicating the process of disaccommodation, validating the choices made during this work.

In this work, a human crystalline lens and its associated structures, i.e., the capsular bag and the zonular fibers, and pseudophakic eyes with a one-piece IOL were built in a FE model. All the models were built based on axisymmetric elements, with linearly elastic isotropic materials, based on the fact that the crystalline lens was a perfectly symmetric structure, around its optical axis. A radial displacement was applied at the tip of the zonular fibers to mimic the movement of the ciliary body during the process of disaccommodation. As there is very few *in vivo* information about all the materials properties, the major part of this work was based on *in silico* studies, about the complete crystalline complex.

In the pseudophakic eye models, the increase of force and stress in the zonules could in fact explain why years after surgery some zonules would break leading to an IOL-capsular bag complex dislocation. This assumption could not be simulated, since there was no information about the tensile strength of the zonules. No variation of parameters in the pseudophakic models, i.e., increase of the Young's moduli of the IOLs, different diameters of capsulorhexis and increased traction force, seemed to have a significant impact on the zonules. It was important to verify their impact on the zonules, since their rupture is the main precursor of IOL-capsular bag dislocation. Since no changes were observed, it was possible to speculate about saying that an axisymmetric model of the pseudophakic eye could be too simplified and that a more realistic geometry of an IOL could have a greater influence on the outcomes of the simulations. More information about the tensile strength of the zonular fibers and the capsular bag would also be crucial to better understand at what point they would break and lead to an IOL dislocation. When studying the influence of the diameter of the capsulorhexis when no traction force was applied at its edge, no change in the stresses of the model proved how important it was to model this traction force and to have *in vivo* information about it, to help building more realistic models.

Some limitations exist in the field, such as few information about all the *in vivo* mechanical properties of all the components of the human lens complex and the real values of traction force exerted in the opening of the capsulorhexis, and it is of extreme importance that new *in vivo* data becomes available in order to further study cataract surgery, its post-operative complication and to find new solutions to avoid them. Regardless of these limitations, no modelling of the eye under cataract surgery like the one proposed here was found

in the literature, turning this work into a complement of the already existing studies about the crystalline complex.

6.3. Future Work

Since this work presented an axisymmetric model, the IOLs built were simplified to represent perfectly axisymmetric lenses, which is not the real configuration of the lens. The geometry of the IOLs could be improved in future works, thanks to 3D models that could replicate different types of asymmetric IOLs (one-piece, three-piece or plate IOLs), in a more realistic way. Moreover, additional parameters could be studied to understand their influence in the overall stresses in all the parts of the models, such as the influence of the gravity, the positioning of the IOL, the type of capsulotomy performed and different densities of zonules (to mimic zonular dehiscence). *In vivo* values of the tensile strength of the zonules and the capsular bag would also have a great impact on the models, since it would be possible to replicate more realistic behaviors in these materials and to know when they would tear. A starting point for the 3D model was first building a replica of the complete human crystalline complex under accommodation and study the stresses throughout the model. In Figure 6.1, the von Mises stress in the capsular bag after disaccommodation of the 3D model are shown.

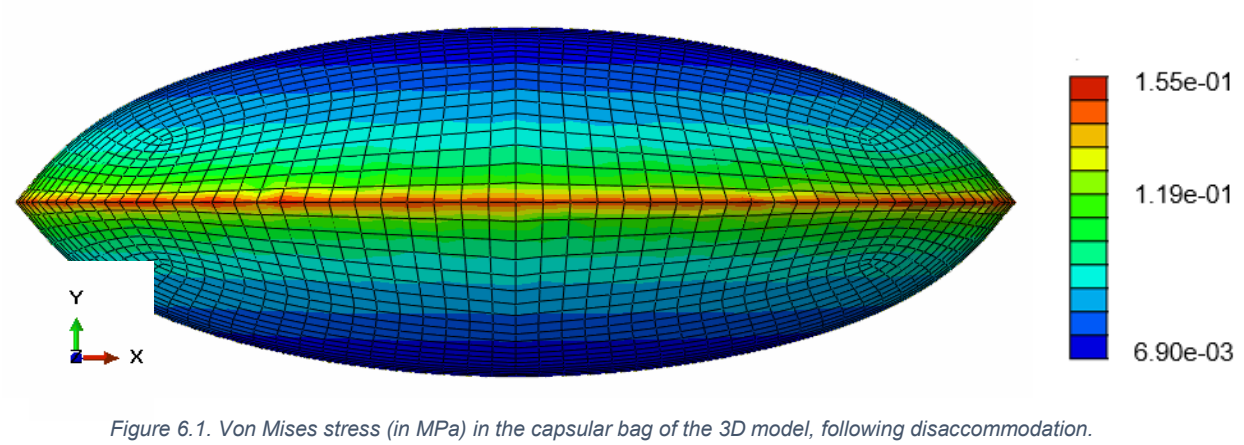

Figure 6.1. Von Mises stress (in MPa) in the capsular bag of the 3D model, following disaccommodation.

In Figure 6.2 an example of a more realistic IOL, in this case a single-piece IOL with a square optic edge, is shown.

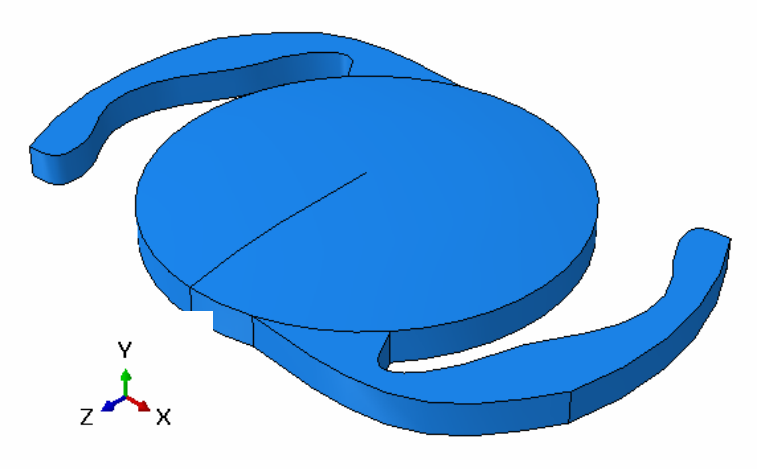

Figure 6.2. Model of a 3D single-piece IOL with a square optic edge.

.

References

Al-Halafi, A. M., Al-Harthi, E., Al-Amro, S., & El-Asrar, A. A. (2011). Visual outcome and complications of pars plana vitrectomy for dislocated intraocular lenses. *Saudi Journal of Ophthalmology*, *25*(2), 187–192. https://doi.org/10.1016/j.sjopt.2011.01.013

Ascaso, F. J., & Huerv, V. (2013). The History of Cataract Surgery. In *Cataract Surgery*. InTech. https://doi.org/10.5772/19243

Bahrami, M., Heidari, A., & Pierscionek, B. K. (2016). Alteration in refractive index profile during accommodation based on mechanical modelling. *Biomedical Optics Express*, *7*(1), 99. https://doi.org/10.1364/BOE.7.000099

Bassnett, S., Missey, H., & Vucemilo, I. (1999). Molecular architecture of the lens fiber cell basal membrane complex. *Journal of Cell Science*, *112 (Pt 1*, 2155–2165.

Bozukova, D., Werner, L., Mamalis, N., Gobin, L., Pagnoulle, C., Floyd, A., … Morris, C. (2015). Double-C loop platform in combination with hydrophobic and hydrophilic acrylic intraocular lens materials. *Journal of Cataract and Refractive Surgery*, *41*(7), 1490–1502. https://doi.org/10.1016/j.jcrs.2014.10.042

Brown, G. C., Brown, M. M., Menezes, A., Busbee, B. G., Lieske, H. B., & Lieske, P. A. (2013). Cataract surgery cost utility revisited in 2012: A new economic paradigm. *Ophthalmology*, *120*(12), 2367–2376. https://doi.org/10.1016/j.ophtha.2013.04.030

Burd, H. J., Judge, S. J., & Cross, J. A. (2002). Numerical modelling of the accommodating lens. *Vision Research*, *42*(18), 2235–2251. https://doi.org/10.1016/S0042-6989(02)00094-9

Burd, H. J., Judge, S. J., & Flavell, M. J. (1999). Mechanics of accomodation of the human eye. *Vision Research*, *39*, 1591–1595.

Cataracts. (2010). *National Eye Institute*. Retrieved from https://www.nei.nih.gov/eyedata/cataract#5

Chien, C. H. M., Huang, T., & Schachar, R. A. (2006). Analysis of human crystalline lens accommodation. *Journal of Biomechanics*, *39*(4), 672–680. https://doi.org/10.1016/j.jbiomech.2005.01.017

Dubbelman, M., Van Der Heijde, G. L., Weeber, H. A., & Vrensen, G. F. J. M. (2003). Changes in the internal structure of the human crystalline lens with age and accommodation. *Vision Research*, *43*(22), 2363–2375. https://doi.org/10.1016/S0042-6989(03)00428-0

Fisher, R., & Pettet, B. (1972). The postnatal growth of the capsule of the human crystalline lens. *Journal of Anatomy*, *112*, 207–214.

Gimbel, H. V., Condon, G. P., Kohnen, T., Olson, R. J., & Halkiadakis, I. (2005). Late in-the-bag

intraocular lens dislocation: Incidence, prevention, and management. *Journal of Cataract and Refractive Surgery*, *31*(11), 2193–2204. https://doi.org/10.1016/j.jcrs.2005.06.053

Goldberg, D. B. (2011). Computer-animated model of accommodation and theory of reciprocal zonular action. *Clinical Ophthalmology*, *5*(1), 1559–1566. https://doi.org/10.2147/OPTH.S25983

Heiting, G. (2017). *Conjunctiva of the Eye*. Retrieved from https://www.allaboutvision.com/resources/conjunctiva.htm

Hermans, E. A., Dubbelman, M., van der Heijde, G. L., & Heethaar, R. M. (2006). Estimating the external force acting on the human eye lens during accommodation by finite element modelling. *Vision Research*, *46*(21), 3642–3650. https://doi.org/10.1016/j.visres.2006.04.012

Hudish, T., Helm, M. L., Patel, A. S., Feldman, B. H., & DelMonte, D. W. (2017). *Anterior Capsular Contraction Syndrome*. Retrieved from http://eyewiki.aao.org/Anterior_Capsular_Contraction_Syndrome

Izak, A. M., Werner, L., Pandey, S. K., Apple, D. J., Vargas, L. G., & Davison, J. A. (2004). Single-piece hydrophobic acrylic intraocular lens explanted within the capsular bag. *Journal of Cataract & Refractive Surgery*, *30*(6), 1356–1361. https://doi.org/10.1016/j.jcrs.2003.09.061

Lanchares, E., Navarro, R., & Calvo, B. (2012). Hyperelastic modelling of the crystalline lens: Accommodation and presbyopia. *Journal of Optometry*, *5*(3), 110–120. https://doi.org/10.1016/j.optom.2012.05.006

Langwińska-Wośko, E., Broniek-Kowalik, K., & Szulborski, K. (2011). The impact of capsulorhexis diameter, localization and shape on posterior capsule opacification. *Medical Science Monitor : International Medical Journal of Experimental and Clinical Research*, *17*(10), CR577-82. https://doi.org/10.12659/MSM.881984

Le, T. (2005). *Nonlinear Finite Element Model Analysis of Human Accommodation Lens*.

Liu, X., Wang, L., Du, C., Li, D., & Fan, Y. (2015). Mechanism of lens capsular rupture following blunt trauma: a finite element study. *Computer Methods in Biomechanics and Biomedical Engineering*, *18*(8), 914–921. https://doi.org/10.1080/10255842.2014.975798

Meacock, W. R., Spalton, D. J., Boyce, J., & Marshall, J. (2003). The effect of posterior capsule opacification on visual function. *Investigative Ophthalmology & Visual Science*, *44*(11), 4665–4669. Retrieved from http://www.ncbi.nlm.nih.gov/pubmed/14578383

Nguyen, J., & Werner, L. (2017). Intraocular Lenses for Cataract Surgery. *Webvision: The Organization of the Retina and Visual System*, (D), 1–20. Retrieved from http://www.ncbi.nlm.nih.gov/pubmed/29437325

Packard, R. (2015). The Evolution of the Capsulotomy. *CRSTEurope*. Retrieved from https://crstodayeurope.com/articles/2015-oct/the-evolution-of-the-capsulotomy/

Prokofyeva, E., Wegener, A., & Zrenner, E. (2013). Cataract prevalence and prevention in Europe: A literature review. *Acta Ophthalmologica*, *91*(5), 395–405. https://doi.org/10.1111/j.1755-3768.2012.02444.x

Pueringer, S. L., Hodge, D. O., & Erie, J. C. (2011). Risk of Late Intraocular Lens Dislocation After Cataract Surgery, 1980–2009: A Population-Based Study. *American Journal of Ophthalmology*, *152*(4), 618–623. https://doi.org/10.1016/j.ajo.2011.03.009

Rusu, I., Chen, Z., Zizva, J., Myung, J. S., & Wald, K. J. (2014). Incidence of cystoid macular edema with iris-fixated posterior chamber intraocular lenses in patients presenting with lens dislocation. *International Ophthalmology*, *34*(5), 1153–1158. https://doi.org/10.1007/s10792-014-9964-2

Schachar, R. A. (1992). Cause and treatment of presbyopia with a method for increasing the amplitude of accommodation. *Annals of Ophthalmology*, *24*(12), 445–447, 452. Retrieved from http://www.ncbi.nlm.nih.gov/pubmed/1485739

Scholtz, S., Kretz, F., & Auffarth, G. (2014). *A Brief History of IOL Materials*. *The Ophthalmologist*. Retrieved from https://theophthalmologist.com/issues/sinister-eclipse/a-brief-history-of-iol-materials/

Sheehan, M. T., Goncharov, A., & Dainty, J. C. (2012). *Eye modelling for personalised intraocular lens design*. https://doi.org/Sheehan2012

Southall, J. P. C. (1962). *Helmholtz's Treatise on Physiological Optics (Volume 3)*. Dover Publications.

Trivedi, R. H., Werner, L., Apple, D. J., Pandey, S. K., & Izak, A. M. (2002). Post cataract- intraocular lens (IOL) surgery opacification. *Eye, Nature Publishing Group*, (16), 217–241. https://doi.org/10.1038/sj/eye/6700066

van Alphen, G. W. H. M., & Graebel, W. P. (1991). Elasticity of tissues involved in accommodation. *Vision Research*, *31*(7–8), 1417–1438. https://doi.org/10.1016/0042-6989(91)90061-9

Wang, K., Venetsanos, D. T., Wang, J., Augousti, A. T., & Pierscionek, B. K. (2017). The importance of parameter choice in modelling dynamics of the eye lens article. *Scientific Reports*, *7*(1), 1–12. https://doi.org/10.1038/s41598-017-16854-9

Weeber, H. A., & van der Heijde, R. G. L. (2008). Internal deformation of the human crystalline lens during accommodation. *Acta Ophthalmologica*, *86*(6), 642–647.

Werner, L., Pandey, S. K., Escobar-Gomez, M., Visessook, N., Peng, Q., & Apple, D. J. (2000). Anterior Capsule Opacification: A Histopathological Study Comparing Different IOL Styles. *Ophthalmology*, (107).

A. Convergence Study for Quadratic Elements

The values of the von Mises stress for each of the nodes, with quadratic elements, versus the number of elements is plotted in **Error! Reference source not found.**. The values were obtained for meshes with global seeds of 0.5, 0.2, 0.1, 0.05 and 0.02.

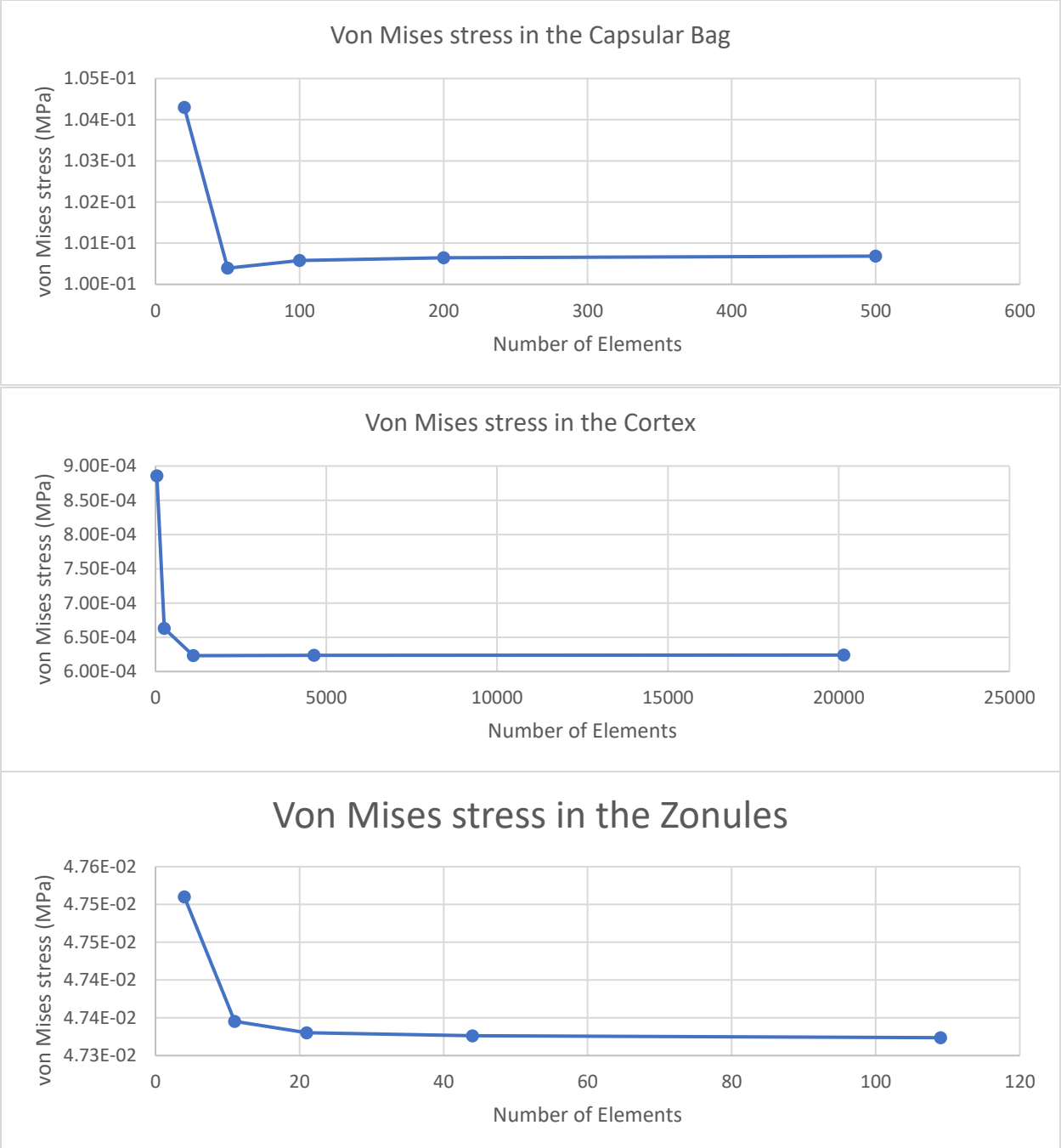

Figure A.1. Values of von Mises stress (MPa) for the nodes in the capsular bag, cortex and zonules, used in the convergence study versus the number of elements for each of those parts.

B. Results of all the Models

In this annex, all the results that were not depicted in Section 5.1 are shown.

Table B.1. Values of von Mises stresses in the zonular fibers, capsular bag and IOL, as well as radial displacement and resulting force at the tip of the zonular fibers for the models M 3.2., M 3.3., M 4.2., M 4.3., M 5.2. and M 5.3.

Model	Variables	Range	Average Value
M 3.2.	S_Z (MPa)	$8.45 \times 10^{-2} – 9.78 \times 10^{-2}$	8.9×10^{-2}
	S_{CB} (MPa)	$1.0 \times 10^{-4} – 3.3 \times 10^{-2}$	1.6×10^{-3}
	S_{IOL} (MPa)	$4.2 \times 10^{-3} – 4.3 \times 10^{-2}$	5.9×10^{-3}
	δ_r (mm)	5.0×10^{-3}	-
	RF_Z (N)	12.9×10^{-2}	-
M 3.3.	S_Z (MPa)	$8.5 \times 10^{-2} – 9.9 \times 10^{-2}$	9.0×10^{-2}
	S_{CB} (MPa)	$3.9 \times 10^{-9} – 2.6 \times 10^{-4}$	9.3×10^{-6}
	S_{IOL} (MPa)	$4.0 \times 10^{-3} – 4.4 \times 10^{-2}$	6.1×10^{-3}
	δ_r (mm)	1.2×10^{-5}	-
	RF_Z (N)	12.9×10^{-2}	-
M 4.2.	S_Z (MPa)	$8.5 \times 10^{-2} – 9.8 \times 10^{-2}$	8.9×10^{-2}
	S_{CB} (MPa)	$5.6 \times 10^{-4} – 1.8 \times 10^{-2}$	2.6×10^{-3}
	S_{IOL} (MPa)	$6.2 \times 10^{-4} – 6.9 \times 10^{-2}$	7.8×10^{-3}
	δ_r (mm)	2.9×10^{-3}	-
	RF_Z (N)	12.9×10^{-2}	-
M 4.3.	S_Z (MPa)	$8.5 \times 10^{-2} – 9.9 \times 10^{-2}$	9.0×10^{-2}
	S_{CB} (MPa)	$2.1 \times 10^{-7} – 3.9 \times 10^{-5}$	5.2×10^{-6}
	S_{IOL} (MPa)	$6.5 \times 10^{-4} – 7.3 \times 10^{-2}$	8.0×10^{-3}
	δ_r (mm)	5.7×10^{-6}	-
	RF_Z (N)	12.9×10^{-2}	-
M 5.2.	S_Z (MPa)	$8.5 \times 10^{-2} – 9.8 \times 10^{-2}$	8.9×10^{-2}
	S_{CB} (MPa)	$3.3 \times 10^{-4} – 5.9 \times 10^{-2}$	2.9×10^{-3}
	S_{IOL} (MPa)	$5.3 \times 10^{-4} – 5.3 \times 10^{-2}$	7.5×10^{-3}
	δ_r (mm)	4.1×10^{-3}	-
	RF_Z (N)	12.9×10^{-2}	-
M 5.3.	S_Z (MPa)	$8.5 \times 10^{-2} – 9.9 \times 10^{-2}$	9.0×10^{-2}
	S_{CB} (MPa)	$7.3 \times 10^{-9} – 2.4 \times 10^{-4}$	1.2×10^{-5}
	S_{IOL} (MPa)	$5.6 \times 10^{-4} – 5.7 \times 10^{-2}$	8.0×10^{-3}
	δ_r (mm)	1.0×10^{-5}	-
	RF_Z (N)	12.9×10^{-2}	-

Table B.2. Values of von Mises stresses in the zonular fibers, capsular bag and IOL, as well as radial displacement and resulting force at the tip of the zonular fibers for the models M 6.2., M 6.3., M 7.1., M 7.2., M 7.3., M 8.2. and M 8.3.

Model	Variables	Range	Average Value
M 6.2.	S_Z (MPa)	$8.5 \times 10^{-2} – 9.8 \times 10^{-2}$	8.9×10^{-2}
	S_{CB} (MPa)	$7.7 \times 10^{-4} – 3.2 \times 10^{-2}$	4.0×10^{-3}
	S_{IOL} (MPa)	$9.7 \times 10^{-4} – 1.3 \times 10^{-1}$	1.2×10^{-2}
	δ_r (mm)	2.2×10^{-3}	-
	RF_Z (N)	12.9×10^{-2}	-
M 6.3.	S_Z (MPa)	$8.5 \times 10^{-2} – 9.9 \times 10^{-2}$	9.0×10^{-2}
	S_{CB} (MPa)	$4.5 \times 10^{-7} – 7.0 \times 10^{-4}$	8.3×10^{-6}
	S_{IOL} (MPa)	$1.0 \times 10^{-3} – 1.3 \times 10^{-1}$	1.3×10^{-2}
	δ_r (mm)	4.5×10^{-6}	-
	RF_Z (N)	12.9×10^{-2}	-
M 7.1.	S_Z (MPa)	$8.5 \times 10^{-2} – 9.8 \times 10^{-2}$	8.9×10^{-2}
	S_{CB} (MPa)	$1.5 \times 10^{-3} – 1.4 \times 10^{-1}$	6.1×10^{-3}
	S_{IOL} (MPa)	$7.8 \times 10^{-4} – 9.6 \times 10^{-2}$	1.2×10^{-2}
	δ_r (mm)	4.8×10^{-3}	-
	RF_Z (N)	12.9×10^{-2}	-
M 7.2.	S_Z (MPa)	$8.5 \times 10^{-2} – 9.8 \times 10^{-2}$	8.9×10^{-2}
	S_{CB} (MPa)	$6.4 \times 10^{-4} – 1.1 \times 10^{-1}$	4.3×10^{-3}
	S_{IOL} (MPa)	$8.0 \times 10^{-4} – 9.8 \times 10^{-2}$	1.2×10^{-2}
	δ_r (mm)	3.4×10^{-3}	-
	RF_Z (N)	12.9×10^{-2}	-
M 7.3.	S_Z (MPa)	$8.5 \times 10^{-2} – 9.9 \times 10^{-2}$	9.0×10^{-2}
	S_{CB} (MPa)	$1.4 \times 10^{-8} – 2.9 \times 10^{-4}$	1.5×10^{-5}
	S_{IOL} (MPa)	$8.3 \times 10^{-4} – 1.0 \times 10^{-1}$	1.3×10^{-2}
	δ_r (mm)	9.1×10^{-6}	-
	RF_Z (N)	12.9×10^{-2}	-
M 8.2.	S_Z (MPa)	$8.5 \times 10^{-2} – 9.8 \times 10^{-2}$	8.9×10^{-2}
	S_{CB} (MPa)	$9.4 \times 10^{-4} – 3.7 \times 10^{-2}$	4.5×10^{-3}
	S_{IOL} (MPa)	$1.2 \times 10^{-3} – 1.5 \times 10^{-1}$	1.4×10^{-2}
	δ_r (mm)	1.9×10^{-3}	-
	RF_Z (N)	12.9×10^{-2}	-
M 8.3.	**S_Z (MPa)**	$8.5 \times 10^{-2} – 9.9 \times 10^{-2}$	9.0×10^{-2}
	S_{CB} (MPa)	$5.5 \times 10^{-7} – 8.2 \times 10^{-5}$	9.5×10^{-6}
	S_{IOL} (MPa)	$1.3 \times 10^{-3} – 1.6 \times 10^{-1}$	1.5×10^{-2}
	δ_r (mm)	4.1×10^{-6}	-
	RF_Z (N)	12.9×10^{-2}	-

Table B.3. Values of von Mises stresses in the zonular fibers, capsular bag and IOL, as well as radial displacement and resulting force at the tip of the zonular fibers for the models M 9.1., M 9.2. and M 9.3.

Model	Variables	Range	Average Value
M 9.1.	S_Z (MPa)	$8.5 \times 10^{-2} – 9.8 \times 10^{-2}$	8.9×10^{-2}
	S_{CB} (MPa)	$1.8 \times 10^{-3} – 1.7 \times 10^{-1}$	6.8×10^{-3}
	S_{IOL} (MPa)	$9.4 \times 10^{-4} – 1.1 \times 10^{-1}$	1.4×10^{-2}
	δ_r (mm)	4.3×10^{-3}	-
	RF_Z (N)	12.9×10^{-2}	-
M 9.2.	S_Z (MPa)	$8.5 \times 10^{-2} – 9.8 \times 10^{-2}$	8.9×10^{-2}
	S_{CB} (MPa)	$7.8 \times 10^{-4} – 1.3 \times 10^{-1}$	4.8×10^{-3}
	S_{IOL} (MPa)	$9.5 \times 10^{-4} – 1.2 \times 10^{-1}$	1.4×10^{-2}
	δ_r (mm)	3.1×10^{-3}	-
	RF_Z (N)	12.9×10^{-2}	-
M 9.3.	S_Z (MPa)	$8.5 \times 10^{-2} – 9.9 \times 10^{-2}$	9.0×10^{-2}
	S_{CB} (MPa)	$8.9 \times 10^{-9} – 3.4 \times 10^{-4}$	1.6×10^{-5}
	S_{IOL} (MPa)	$9.9 \times 10^{-4} – 1.2 \times 10^{-1}$	1.4×10^{-2}
	δ_r (mm)	8.6×10^{-6}	-
	RF_Z (N)	12.9×10^{-2}	-